Immuno-Responsive Gene-1: A mitochondrial gene regulates pathogenic Th17 in CNS autoimmunity mouse model

Mohammad Nematullah[1], Mena Fatma[1], Faraz Rashid[1], Kameshwar Ayasolla[1], Mohammad Ejaz Ahmed[1], Sajad Mir[1], Insha Zahoor[1], Ramandeep Rattan,[2] and Shailendra Giri[1]

[1]Department of Neurology, [2]Division of Gynaecology Oncology, Department of Women's Health Services, Henry Ford Hospital, E&R Building, Room 4051, Detroit, USA

Running Title: *Irg1* negatively regulates autoreactive CD4 T cells in EAE

Keywords: *Irg1*, Th17, EAE, Multiple sclerosis, GM-CSF, IL17a, IFNγ, IL1β, NLRP3

To whom correspondence should be addressed:

Shailendra Giri, PhD

Senior Scientist
Department of Neurology,
Henry Ford Hospital,
2799 W Grand Blvd,
Detroit, Michigan, 48202, USA

Office: (313) 916-7725
Fax: (313) 916-7250
Email: SGiri1@hfhs.org

Abstract

Pathogenic Th17 cells are crucial to CNS autoimmune diseases like multiple sclerosis (MS), though their control by endogenous mechanisms is unknown. RNAseq analysis of brain glial cells identified immuno-responsive gene 1 (*Irg1*), a mitochondrial-related enzyme-coding gene, as one of the highly upregulated gene under inflammatory conditions which were further validated in the spinal cord of animals with experimental autoimmune encephalomyelitis (EAE), an animal model of MS. Moreover, *Irg1* mRNA and protein levels in myeloid, CD4, and B cells were higher in the EAE group, raising questions about its function in CNS autoimmunity. We observed that *Irg1* knockout (KO) mice exhibited severe EAE disease and greater mononuclear cell infiltration, including triple-positive CD4 cells expressing IL17a, GM-CSF, and IFNγ. Lack of *Irg1* in macrophages led to higher levels of Class II expression and polarized myelin primed CD4 cells into pathogenic Th17 cells through the NLRP3/IL1β axis. Our findings show that *Irg1* in macrophages plays an important role in the formation of pathogenic Th17 cells, emphasizing its potential as a therapy for autoimmune diseases, including MS.

Introduction

Multiple Sclerosis (MS) is an autoimmune disorder of the Central Nervous System that mostly affects young individuals. It is primarily influenced by autoreactive CD4+T cells, which are responsible for the demyelination process. An imbalance in the delicate regulation of innate and adaptive immune responses occurs in the context of MS, leading to changes in the presentation of self-antigens to CD4+T cells by antigen-presenting cells (APCs) [1,2]. In the initial phase of the disease, both dendritic cells and macrophages function as local antigen presenters for CD4+T cells, facilitating the development of T-cells towards Th1/Th17 states. These Th cells are characterized by the production of cytokines such as IFNγ, IL17a, and GMCSF. These effector T helper cells enter the central nervous system (CNS) and are subsequently stimulated by local antigen-presenting cells (APCs) such microglia, resulting to the demyelinating [3,4].

The production of few immuno-metabolites is strictly controlled and occurs exclusively under inflammatory conditions. One such metabolite, itaconate, an offshoot metabolite of TCA, is recognized for its antibacterial properties and is closely associated with bacterial infection such Mycobacterium tuberculosis[5]. Immune-Responsive Gene 1 (*Irg1*) is a mitochondrial enzyme that produces itaconate in high concentrations (milli-molar) during inflammatory conditions, primarily in myeloid lineage cells [6]. Itaconate is recognized for its antibacterial activities and ability to suppress the immune system, suggesting that the regulation of immune cell activity is a significant feature of itaconate [7-9].

Itaconate has been found to decrease the oxygen consumption rate, and additionally, it inhibits the activity of Succinate Dehydrogenase (SDH), leading to increased levels of succinate in activated macrophages [10,11]. Furthermore, studies have demonstrated that *Irg1* acts as the intermediary between the innate and adaptive immune responses[12]. Its absence exaggerated pro-inflammatory responses, tissue damage and recruitment of inflammatory cells [8]. Itaconate has been documented to provide protection against autoimmune disease by regulating neuroinflammation[13] and restoring the balance of T cells through metabolic and epigenetic reprogramming in experimental autoimmune encephalomyelitis (EAE) [14]. Nevertheless, the impact of *Irg1* in regulating CNS autoimmunity has not been investigated. The current work aimed to examine the impact of *Irg1* on the progression of EAE and assess its potential in controlling T-cell differentiation by using *Irg1* global knock out (KO) mice. Our observation revealed that loss of *Irg1* led to significant alteration in the body natural defense system, resulting in higher EAE severity. As we observed aberrant expression of autoreactive triple positive CD4 cells expressing IL17, GMCSF and IFNγ in the central nervous system, suggesting *Irg1* expression is a crucial regulator of CD4 cells functioning. Furthermore, macrophages lacking *Irg1* showed increased

ability to present antigens and induced the polarization of Th17 cells through the NLRP3/IL-1β pathway. The study revealed *Irg1* as a specific target for therapeutic intervention in the treatment of MS.

Results

Induction of itaconate and *Irg1* in immune cells and spinal cord during EAE

Previously we have reported altered metabolic signature in the blood of MS patients, chronic and relapsing-remitting mouse models of EAE using untargeted global metabolic profiling [15-18], documenting the blood based alteration in metabolism during MS or EAE disease [19]. To examine if metabolic genes are perturbed in brain glial cells under inflammatory conditions, we generated rat brain primary mixed glial cells and treated them with LPS/IFNγ (0.5 µg/ml and 20 ng/ml) for 8 hours and processed for RNAseq. Interestingly, our results showed *Irg1* as among the top ten genes with the highest fold change (padj-6.30E-09, logFC-9.9) (**Fig. 1A**). We validated the levels of *Irg1* at various time points and found that LI induced the expression of *Irg*1 at 4h and peaked at 8h, which was reduced at 16h of treatment (**Fig 1B**). To replicate the *in vitro* finding of higher *Irg1* levels under inflammatory condition, we examined its expression in the spinal cord of EAE. We observed that *Irg1* expression at protein levels is induced significantly in spinal cord of EAE compared to CFA control which is reflected by immunohistochemistry in the spinal cord section (**Fig. 1C-D**). Since *Irg1* has been reported to be increased in immune cells during infection or inflammation, we examined its expression in various cell types including CD11b, monocytes, CD4 and B cells during EAE disease. Expression of *Irg1* in these isolated immune cells was higher during EAE compared to CFA control which was further validated by quantitative PCR (**Fig 1E-F**). Interestingly, we also observed the significant upregulation of Irg-1 at both mRNA and protein level in $CD4^{+}$T of EAE mice compared to control mice, earlier reports mainly about the Irg-1 expression in myeloid cells[12,20]. These sets of experiments suggest that itaconate levels are increased as a results of higher *Irg1* expression in CNS during EAE, raising the question, if their elevated levels are protective or pathogenic.

Loss of *Irg1* led to severe EAE and activation of immune cells

To evaluate that the significance of elevated *Irg1* expression in the spinal cord in EAE, we induced EAE in global *Irg1* knockout (KO) mice using MOG_{35-55} (200 µg/ml) as described before. We observed a significant severity in the clinical score and cumulative score in *Irg1* KO mice compared to Wt mice (**Fig. 2A-B**). Upon examining antigen specific response, spleen/lymph nodes cells of *Irg1* KO produced signficantly higher levels of IFNy, IL17a and GM-CSF without

affecting IL4 upon MOG_{35-55} stimulation (**Fig 2C**). Further, the histopathology analysis showed a higher inflammatory cell infiltrates and demyelination in the spinal cord of *Irg1* KO mice as revealed by H&E and LFB staining, respectively, compared to Wt (**Fig. 2D**) which correlates well with severity of clinical score in *Irg1* KO mice. Infiltration of mononuclear cells, including myeloid cells and T cells that inflame the CNS environment, is detrimental for oligodendrocytes and neurons, leading to demyelination in MS and EAE [21]. Like H&E staining data, we also observed a significant increase in the infiltrating mononuclear cells ($CD45^{hi}$ populations) in the CNS tissue of *Irg1* KO mice with EAE compared to Wt EAE (**Fig. 2E**). Immune profiling followed by tSNE projection in the CNS infiltrates at the peak of the disease showed a higher number of CD4 cells in *Irg1* KO compared to Wt. Hence, we quantified the absolute number of infiltrating CD4 cells ($CD45^{+}CD3^{+}CD4^{+}$) and found that *Irg1* KO mice with EAE exhibited ~3 fold higher CD4 cells compared to Wt (**Fig 2G**). CNS infiltrates in *Irg1* KO exhibited higher levels of Th1, Th17 expressing double positive CD4 (expressing IL17 and GM-CSF) and triple positive CD4 expressing IL17, GM-CSF and IFNγ compared to Wt infiltrating cells (**Fig 2I**). Since myeloid cells are important for disease induction and severity of disease due to their role in differentiating antigen specific Th cells in the peripheral lymphatic organ and within CNS as well [2], we profiled myeloid in Wt and KO CNS tissue. Myeloid cell profiling by tSNE projection in the CNS infiltrates revealed a higher infiltration of CD11b+ve myeloid cells, monocytes/macrophage and dendritic cells (DC) (**Fig 2F, 2J**). Similar observation was seen in spleen as significant increment in two different macrophage populations including $CD11b^{low}F4/80^{+}$ (red pulp macrophages)[22] and ($CD11b^{med}F4/80^{+}$ (migrated macrophages) was observed (**Fig S1-2**).

CD4 cells lacking *Irg1* are highly pathogenic in nature

As mentioned above, we observed that CD4 lacking *Irg1* exacerbated the expression of inflammatory cytokines (IL17a, GM-CSF and IFNγ), therefore, next, we intended to know if antigen specific CD4 cells lacking *Irg1* are encephalitogenic in nature. We performed adoptive transfer (Adt) of MOG_{35-55} primed CD4 cells lacking *Irg1* and Wt into Wt B6 mice. For this, we immunized Wt and *Irg1* KO mice with MOG_{35-55} and post 10 days, spleen/LNs cells were stimulated with antigen in the presence of anti-IFNγ (10 µg/ml) and IL12p70 (20 ng/ml). Post 72h, we found that CD4 lacking *Irg1* produced higher levels of IL17a, and GM-CSF compared to Wt CD4 cells (**Fig 3A**). Upon adoptive transfer of these cells in Wt mice, we found that Wt mice receiving MOG-primed CD4 cells lacking *Irg1* showed severe EAE pathogenicity compared to Wt mice receiving MOG-primed Wt CD4 cells (**Fig. 3B**). Furthermore, Rag1 mice, which is deficient in resident T and B cells, also showed severe EAE pathogenicity upon Adt of MOG_{35-55}-primed CD4 lacking

Irg1 (KO->Rag1) compared to Wt CD4 cells (Wt->Rag1) (**Fig. 3C**). Severity of clinical symptoms in KO->Rag1 are reflected due to significantly higher infiltration of CD4 cells in CNS with Th17 phenotype. Although we did not observe significant but trending increment in the population of CD4 expressing IFN-γ^+ and GMCSF$^+$ populations with no change in Th2 cells in the CNS of KO->Rag1 compared to Wt->Rag1 group (**Fig. 3D-H**). More importantly, there was exacerbation of double (CD4$^+$IL17$^+$GMCSF$^+$ and CD4$^+$IL17$^+$IFN-γ^+) and triple (CD4$^+$IL17$^+$GMCSF$^+$IFNγ^+) positive cells in the CNS of KO->Rag1 to Wt->Rag1 group with EAE (**Fig. 3I-K**). These sets of data clearly suggest that CD4 cells lacking *Irg1* are highly pathogenic in nature and the expression of *Irg1* may be one of the crucial regulators of CD4 mediated pathogenicity in autoimmune diseases like EAE.

***Irg1* KO potentiates the pathogenic Th17 subsets upon EAE induction**

Th17 subset is critical to EAE progression, are known to have two distinct subsets depending on their pathogenic inflammatory profile [23]. One is known as pathogenic Th17 (pTh17) subset which produces high level of inflammatory mediatory such as IL17a and GMCSF and induce EAE disease [24-26], while second one is non-pathogenic Th17 (npTh17) which has very mild inflammatory profile [27,28]. Since we observed CD4 lacking *Irg1* exhibited higher Th17 in number with encephalitogenic properties, we examined if CD4 lacking *Irg1* expression predisposed to pathogenic Th17 phenotype. For this, we cultured naive CD4 cells from Wt and *Irg1* KO and cultured in the condition of npTh17 (TGFβ and IL6) and pTh17 (TGFβ, IL6, IL23 and IL1β) conditions as described before [23]. We observed that CD4 cells lacking *Irg1* produced significantly higher levels of IL17a in both, pathogenic and non-pathogenic conditions (**Fig. 4A**). This observation was further supported by intracellular staining depicting higher number of IL17-producing Th17 *Irg1* KO CD4 cells in both condition (**Fig. 4B**). A set of differentially expressed genes specific to pTh17 and npTh17 phenotype [23] were examined and we observed a significantly higher upregulation of genes associated with pathogenic Th17 including RORγt, CSF2, CCl3 and LAG3 in CD4 cells lacking *Irg1* compared to Wt CD4 cells with downregulation of genes associated with non-pathogenic Th17 such as CD5L and IL-9 (**Fig. 4C**) Although we found upregulation of some genes associated with non-pathogenic Th17 such AHR and MAF-1 in CD4 cells lacking *Irg1*, appealingly, the AHR and MAF-1 genes are reported to be associated with proliferation of Th17 cells. These results suggesting that *Irg1* could be negatively regulating both pathogenicity as well as proliferation of Th17 subsets. Th17 differentiation is programmed by nuclear factor, retinoid-related orphan receptor-gamma (RORγ)[29,30]. As depicted from **figure 4C & D**, CD4 lacking *Irg1* expression expressed a higher level of RORγ compared to Wt CD4 under

npTh17 and pTh17 condition. To clarify detailed mechanism, we used CHIP assay to establish whether increased levels of RORγ in CD4 cells lacking *Irg1* is responsible for pathogenic Th17 phenotype. We found that recruitment of RORγ is significantly higher in the promoter of IL17a of CD4 lacking *Irg1* compared to Wt CD4 cells (**Fig. 4E**). Rabbit IgG was used as a negative control and no PCR product could be seen suggesting the specificity of CHIP assay. This set of data clearly suggests that *Irg1* negatively regulates RORγ expression and its recruitment to influence the Th17 cell differentiation and pathogenicity.

Irg1 **lacking macrophage are proinflammatory in nature**

Myeloid cells mainly monocytes/macrophages are the major effectors of demyelination in both MS and EAE[31-33]. A study reported that macrophage lacking *Irg1* showed hyperinflammatory response after mycobacterium infection[8]. Here we examined the status of proinfammatopry cytokines expression in Wt and *Irg1* KO macrophage. We found that macrophage lacking *Irg1* exhibited higher expression of TNFα, IL6, IL1β and MCP1 under inflammatory condition (LPS treatment) compared to Wt macrophage (**Fig 5A**). Similar results were observed when splenic macrophage were isolated from spleen (anti-F4/80 microbeads, Miltenyi Biotec) of Wt and *Irg1* KO EAE and their expression were examined using qunatitaive PCR (**Fig. 5B**). Furthermore, qPCR revealed that *Irg1* KO BMDM showed significant upregulation in iNOS expression, while a differential effect was observed in anti-inflammatory associated genes such as increment in EGR2 and decrement in Arg1 compared to Wt BMDM with no change in CD206 (**Fig. S3**). Macrophages are known for phenotypic transitions, therefore, to elaborate the impact of *Irg1* loss on their phenotypic transitions, BMDM were stimulated with IFNγ (50ng/ml) and phenotypic characterization was performed using flow cytometry. We found that *Irg1* KO BMDM were significantly pushed towards pro-inflammatory state, as characterized by $F4/80^{+}CD86^{+}$ and $F4/80^{+}ClassII^{+}$ compared to Wt BMDM (**Fig 5C**). Observed higher proinflammatory cytokines (IL6 and IL1β) are well known to potentiate and maintain Th17 phenotype[34] suggesting the higher expression of IL17 in *Irg1* KO EAE could be due to the higher levels of these cytokines.

Loss of ***Irg1*** **showed high antigen presentation capability of macrophages**

To further confirm that infiltrated *Irg1* KO macrophage are proinflamatory in CNS, we profiled infiltrated macrophages expressing Class II in *Irg1* KO and Wt with EAE. We found that expression of both Class II was significantly upregulated in infiltrated macrophage ($CD11b^{+}F4/80^{+}$ cells) compared to Wt (**Fig. 5D**). We also examine the class II expression on other infiltrating myeloid cells in Wt and *Irg1* KO mice with EAE. The tSNE projection of Class II+ve CD45 infiltrated myeloid

cells revealed that all myeloid cells including CD11b+ve, Ly6C+ve monocytes, CD11c+ve and macrophage (F4/80) exhibited higher Class II expression in *Irg1* KO compared to Wt (**Fig. 5E**). We further immune-profile specific cell population and found that infiltrating inflammatory dendritic cells (DC; CD45+CD11b-CD11c+ClassII+), monocytic DC (CD45+CD11b+CD11c+), monocytes (CD45+CD11b+Ly6G$^-$Ly6C+) and brain resident microglia (CD45^{lo}CD11b+) were shown to expressed higher levels of Class II in *Irg1* KO mice compared to Wt with EAE (**Fig. 5F**) suggesting their potential as antigen presenting ability to myelin specific CD4 cells. Also, a similar trend was found in splenic macrophages (**Fig. S1-2**).

To test this hypothesis, we generated macrophages from bone marrow from both Wt and *Irg1* KO mice and co cultured with 2D2 CD4 cells in the presence of MOG_{35-55} and examined the production of pro-inflammatory cytokines by ELISA and phenotypic characterization through flow cytometry. We observed that 2D2 CD4 cells co-cultured with *Irg1* KO macrophages showed significantly higher levels of IL17a, GM-CSF and IFNγ (**Fig. 6A-B**) compared to Wt macrophage cocultured with 2D2 CD4 cells. Similar observations were found when CD4 cells were processed for intracellular staining for IL17a, GM-CSF and double positive (CD4+IL17a+GM-CSF+) (**Fig. 6C**). These sets of experiments clearly demonstrate that loss of *Irg1* potentiate macrophage ability to present antigen efficiently to myelin specific CD4 cells and polarized them into Th17 phenotype expressing GM-CSF.

Monocytes/Macrophages are the major producer of IL1β in *Irg1* KO mice

It is known that myeloid cells are the main source of IL1β production, which is a key player in polarizing pathogenic Th17 [35,36]. Since *Irg1* lacking macrophage produced higher levels of IL1β and other studies have reported similar outcome, we postulated that IL1 β is driving pathogenic Th17 phenotype in *Irg1* KO. First, we determine which myeloid population is the major contributor of IL1β in brain filtrating cells (BILs) of Wt and *Irg1* KO using tSNE plots and found that macrophage (F4/80+ve population) and CD11c+ve cells are major producer in BILs of Wt and *Irg1* KO (**Fig. 7A**). Among them, macrophages lacking *Irg1* significantly produced higher levels of IL1β (**~2 fold**) compared to Wt reflected in bar graph and heat map (**Fig. 7B-D**). Since microglia is known as a brain-resident macrophage and plays a key role in neuroinflammation[37,38], we also examine its contribution in producing IL1β in *Irg1* KO with EAE. We observed that *Irg1* lacking microglia produced significantly higher IL1β compared to Wt microglia (**Fig. 7E-H**). Immunophenotyping revealed that other myeloid population including infiltrated myeloid cells (CD11b$^+$CD45^{hi}), classical monocytes (CD11b$^+$CD45$^+$Ly6C^{high}) and infiltrated macrophage (CD11b$^+$F4/80$^+$) were significantly higher in producing IL1β producing in CNS of *Irg1* KO

compared to Wt with EAE (**Fig. 7E-H**). Additionally, both red pulp splenic macrophages and migrated macrophages showed significant increment in the production of IL1β in *Irg1* KO compared to Wt with EAE (**Fig. S1-2**). Through these observations, we concluded that lack of *Irg1* led to upregulation of macrophage/monocytes producing pro-inflammatory cytokines mainly IL1β that possibly push myelin specific CD4 T cells towards pathogenic Th17 cells.

***Irg1* negatively regulates inflammasome in macrophages during EAE**

IL1β is a NLRP3 inflammasome dependent cytokine and NLRP3 have been reported to play a critical role in the development of EAE by regulating Th17 [39] and chemotactic immune cell migration [40]. Since we found higher level of IL1β in *Irg1* KO mice with EAE and *Irg1* negatively regulates NLRP3 activity[41,42] in macrophages, we examined NLRP3 inflammasome components. For this, Wt and *Irg1* lacking macrophage were treated with LPS for 6h and cell lysate was processed for including IL1β, NLRP3, ASC and GSDMD using immunoblot analysis. As depicted in **figure 8A**, *Irg1* lacking macrophage produced higher levels of pro-IL1β and cleaved IL1β compared to Wt macrophage under LPS stimulation. Similar to IL1β, *Irg1* lacking macrophages expressed higher levels of NLRP3 and GSDMD without any change in the levels of ASC suggesting that NLRP3 inflammasome is higher. Higher levels of IL1β and NLRP3 were further validated using qPCR. As depicted in **figure 8B**, stimulation of Wt macrophage with LPS induced the expression of IL1β and NLRP3 which were significantly heighten in *Irg1* lacking macrophages under LPS stimulation suggesting that *Irg1* negatively regulates NLRP3 and IL1β in macrophages.

As we already demonstrated that *Irg1* KO mice exhibited higher pTh17 CD4 cells compared to Wt mice with EAE, in which IL1β expression plays an important role in pTh17 differentiation[35,36], therefore, to further understand the importance of IL1β toward *Irg1* mediated Th17 pathogenicity, we co-cultured *Irg1* KO macrophages with myelin-specific CD4 cells with either IgG or αIL1β neutralizing antibody (10μg/ml). We observed that neutralization of IL1β significantly diminished the population of IL17-A^{+}, GMCSF^{+}, and double positive population (IL17^{+}GMCSF^{+}) compared to IgG alone (**Fig. 8C**) where *Irg1* KO macrophage were cocultured with antigen-specific CD4 cells. Our observations suggested that *Irg1* negatively regulates IL1β in macrophages which plays critical role in differentiating pTh17 CD4 cells resulting in severity of EAE clinical symptoms in *Irg1* KO mice.

Discussion

The abundance of pathogenic CD4 cells is an important characteristic of both MS and EAE [43]. However, the process by which naïve CD4 T cells transform into pathogenic Th17 cells remains unclear. The current study provides evidence that *Irg1*, a mitochondrial enzyme responsible to produce itaconate, plays a significant role in the pathogenicity of Th17 CD4 cells in EAE. There are few studies reporting the immune-regulatory impact of *Irg1*[8,44], our present study demonstrated that *Irg1* is an important regulator of natural defense mechanisms. However, recent studies have shown that the introduction of itaconate can reduce the course of EAE [13,14]. Nevertheless, the extent to which *Irg1* contributes to the control of immune cells in the context of EAE disease remains uncertain.

Irg1 is a mitochondrial enzyme that is highly upregulated during infection [8], which is consistent with our observation of increased expression at both the mRNA and protein levels in several types of activated immune cells, such as CD11b myeloid cells, monocytes, B cells, and CD4 T cells. Considering that itaconate, a product of *Irg1*, has been shown to provide protection against EAE disease by reducing neuroinflammation[13] and altering the metabolic and epigenetic programming of T cells[14]. While the impact of itaconate on the metabolic regulation of Th17 and Treg balance has been documented, the expression of *Irg1* in CD4 T cells has not been documented. The majority of the research has mostly examined the myeloid-centric function of *Irg1* in inflammation. However, our findings indicate that its expression is elevated in CD4 and B cells during EAE, as compared to CFA. This raises the question of whether *Irg1* has a protective or harmful role in autoimmune diseases like MS. In the future, we will investigate the cell-specific role of *Irg1* in CNS autoimmunity in CD4 or B cells. However, our current findings indicate that *Irg1* plays a crucial role in regulating macrophages as antigen presenting cells with a hyperinflammatory phenotype. *Irg1* knockout mice upon EAE induction exhibited heightened inflammation and demyelination in comparison to Wt mice with EAE. It is well known that alteration in Immune cells comprising altered phenotypic states, functional states as well as altered metabolic states are identified major culprits of EAE progression [43]. The metabolic alterations in macrophages of CD4 cells were not the focus of this investigation. However, future studies will be designed to specifically investigate these changes.

Given that the infiltration of macrophages into the central nervous system (CNS) is a key characteristic of multiple sclerosis (MS)[43,45], our observations indicate a noteworthy increase in the infiltration of circulating monocytes and macrophages into the CNS in *Irg1* KO compared to Wt. This suggests that the expression of *Irg1* plays a crucial role in the infiltration of immune cells in EAE. In addition, *Irg1* KO mice exhibited disease severity and macrophages lacking *Irg1*

displayed heightened production of pro-inflammatory cytokines, suggesting that *Irg1* impacts the functional states of immune cells as well as involves in EAE pathogenicity. Our results align with previous studies, which showed that macrophages lacking *Irg1* exhibited a proinflammatory macrophage phenotype[8,46,47]

Our study has discovered a significant mechanism by which *Irg1* suppresses the inflammatory response and ability of macrophages to present antigens. This is achieved through the activation of the NLRP3-IL1β cascade, which regulates the pathogenic Th17 cell and ultimately controls CNS autoimmunity. However, we have not investigated the role of metabolic regulation mediated by *Irg1* in this mechanism. The induction of *Irg1* in different cell types during EAE appears to be an innate defensive mechanism aimed at regulating inflammation and the course of the disease. While the levels of itaconate significantly increased in immune cells and in the spinal cord during EAE disease, it remains uncertain if its concentration exceeds the threshold required to effectively regulate inflammation and restore the mobility. It has been reported that itaconate can elevate the levels of IFN-β. Additionally, it has been observed that *Irg1* KO macrophages produce significantly lower levels of IFN-I and its downstream gene expression related to type I IFN signaling, compared to Wt macrophages [48]. This suggests that itaconate could potentially be another contributing factor to the increased severity observed in *Irg1* KO with EAE, which has not been thoroughly investigated.

In the present study, we observed that the loss of *Irg1* led to aberrant expression of double positive ($IL17a^{+}IFN\gamma^{+}$) as well as triple positive ($IL17A^{+}IFN\gamma^{+}GM\text{-}CSF^{+}$) cells which are known to be antigen specific CD4 T cells population and highly pathogenic in nature [49,50]. Antigen Presentation is one of the crucial mechanisms that involves in $CD4^{+}$ T derived immune response [51], although the pathophysiology of MS is still not entirely understood but it is well known that antigen presentation and the immune response play a critical role in EAE disease progression [43,45,52]. Our co-cultured studies with *Irg1* KO macrophages with MOG-primed CD4 cells clearly demonstrated that macrophages lacking *Irg1* expression promoted the development of pathogenic Th17 phenotype compared to Wt macrophages. Th17 cells, a subset of T helper cells that contribute to the immune response against infections and autoimmunity[53], can be categorized as either pathogenic or non-pathogenic based on the type of response they generate and the cytokines they interact with. Pathogenic Th17 cells, which are mainly mediated by IL-1β and IL23 cytokines, play a role in the development of MS by generating pro-inflammatory cytokines and recruiting other immune cells to the site of inflammation, while Non-pathogenic Th17 cells, which devoid of involvement of IL-1β and IL23, shows mild inflammatory response. We observed that splenic macrophages of *Irg1* KO mice showed upregulation in pathogenic Th17 genes while

downregulation in non-pathogenic Th17 genes, indicating that the expression of *Irg1* may play a regulatory role in controlling differentiation of Th17 cells. Our research revealed a significant increase in the population of IL-1β positive cells in both resident and infiltrating macrophages in *Irg1* KO mice compared to Wt mice. IL-1β, which is produced by myeloid cells, is a critical cytokine for the development of pathogenic Th17 cells [54,55]. Our findings are consistent with earlier reports that have extensively documented the significant involvement of IL-1β in CNS inflammation, which has been implicated in the progression of neurological disorders such multiple sclerosis and Alzheimer's disease [56-58]. Immune cells including macrophages, microglia and astrocytes produce IL-1β [59], that activates resident immune cells, recruits immune cells from the periphery, and increases the production of additional pro-inflammatory cytokines in the CNS,, thus amplifying the inflammatory reaction.

The production of cleaved IL-1β is regulated by the cleavage of Procaspase-1 into active Caspase-1, mediated by the activated NLRP3[60]. The increased expression of IL1β in *Irg1* lacking macrophages is consistent with the elevated levels of NLRP3 at both the mRNA and protein levels, as compared to Wt macrophages, suggesting that *Irg1* plays a function in regulating the NLRP3 inflammasome, which is corroborated by earlier findings [41,61]. Antigen presentation and NLRP3 activation have been strongly correlated, leading to the regulation of CD4 T and CD8 T immune response [62-64]. Our findings indicate that IL-1β alone can induce the development of pathogenic Th17 cells in *Irg1* KO cells. Additionally, blocking IL-1β limits the differentiation of CD4 cells into pathogenic Th17 cells, suggesting that *Irg1* is involved in the antigen presentation process of *Irg1*-deficient macrophages in the NLRP3-IL-1β dependent cascade. The aberrant expression of NLRP3 is causing severe inflammatory conditions, an increase in the ability of cells to present antigens, dysfunctions in mitochondria, and a failure in the resolution process such as efferocytosis [63,65]. Based on our current data, we have concluded that *Irg1* regulates the Th17-mediated EAE disease progression in a manner that depends on NLRP3-IL-1β cascade. Collectively, our study suggests that the expression of *Irg1* is a crucial target to regulate phenotypic as well as functional activity of both myeloid and lymphoid cells in progression of EAE, suggesting that targeting *Irg1* could be a promising approach to reduce the severity of MS.

Acknowledgments

This work is in-part supported by research grants from the US National Institutes of Health (AI144004, NS112727), National Multiple Sclerosis Society (US) (RG-2111-38733), and Henry Ford Hospital Internal support (A10270, A30967) to SG. The funders had no role in study design, data collection, and interpretation, or the decision to submit the work for publication.

Author Contributions

MN performed experiments and wrotethe manuscript, MF, FR, KA, MEA performed experiments and finalized the manuscript, SM, IZ and RR analyzed data and finalized the manuscript, SG conceive the idea, directed the study, designed experiments, and finalized the manuscript.

Declaration of interest

The authors declare no competing interests.

Materials and Methods

Animals and Induction of EAE

Breeding pair of Wild type (Wt) and *Irg1* KO were purchased from Jackson Laboratory and maintained in Institutional animal facility. All animal experiments were approved by the Institutional Animal Care and Use Committee of Henry Ford Health, Detroit, MI. All mice were housed and bred in the departmental animal facility with controlled humidity, temperature and 12h:12h light/dark cycle with free access to food and water. On day 0, both Wt and *Irg1* KO mice were immunized by giving subcutaneous injection of 200µl emulsion containing MOG_{35-55} peptide. Pertussis toxin (200 ng/mouse) was injected into mice on day 0 and 2 post immunization. Also, there were one separate set of mice (CFA control group) was administered with incomplete Freund's adjuvant (CFA). Disease scoring in mice was done blindly as described before [17,18,66,67] by using traditional EAE scoring method; 0 = no disease, 1 = complete loss of tail, 2 = partial hind limb paralysis, 3 = complete hind limb paralysis, 4 = complete hind limb and forelimb paralysis, and 5 = dead.

Primary brain rat glial culture: The timed pregnant rat was purchased from Charles River Laboratory. The brains of 2-3-day old rat female and male pups were used to prepare mixed glial cell cultures. We followed our previously published protocol to prepare the primary mixed glial cell culture [67]. Post 10 days of culture, cells were treated with LPS (0.5 µg / ml) + IFNγ (20 ng / ml) to induce inflammatory condition for our study. After 8h of treatment, cells were processed for RNA isolation and RNAseq as described below.

RNA-seq: We extracted total RNA from rat mixed glia stimulated with LI 8 hrs in serum free DMEM media with three replicates. All samples displayed a high RNA Integrity Number (RIN) averaging around 8.90 ± 0.25. PolyA-enriched RNA libraries were prepared with unique barcoding for multiplexing and were sequenced using Novogene services. The STAR aligner was used for alignment. We uniquely mapped paired-end reads of 150bp to the rat reference genome, achieving an approximate mapping rate of 80%. Subsequently, the STAR aligner was utilized for count calling for each sample. For differential expression analysis, we employed the limma-Voom package in R, with a padj cutoff of 0.0005 and a log-fold change (logFC) threshold of 1.5. Additionally, to filter out genes with low expression levels, we set a threshold of 0.1 counts per million (CPM) in at least 80% of the samples. For count normalization, we used the trimmed mean of M-values (TMM) method. Finally, R was used to generate the plots for visualization.

Immunohistochemistry

Mice were anesthetized with Isoflurane and transcardially perfused with 0.9% saline followed by 4% paraformaldehyde in 0.1M phosphate buffer. Brains were removed, post-fixed overnight in paraformaldehyde and cryoprotected in 30% sucrose at 4°C until sank. Coronal sections (25 µm) were cut on a cryotome (Thermo CS3472M0402 Warrington UK) and tissue was collected for histological assessment. Diaminobenzidine (DAB) immunostaining were done by blocking section with 1% BSA in PBS for 1 h at room temperature, followed by incubating with polyclonal anti-*Irg1* antibody (1: 250, CST 19857, cell signaling) overnight at 4°C. The sections were washed three times with 0.1% PBST. Sections were washed and incubated with biotinylated secondary antibody for 30 min at room temperature. Followed by stain were develop by using VECTASTAIN Elite ABC system manufacturer instruction (Vector Laboratories, Burlingame, CA). Sections were washed three times and mounted with mounting medium and covered with glass cover slip. The images were scanned with Aperio eSlide Manager, Leica biosystem). Quantification was performed by using ImageJ software (Version 1.49; NIH, USA). Data were used as means ± SEM.

Isolation and characterization of Brain Infiltrating Cells (BILs)

The Percoll-density gradient was used to isolate BILs from CNS tissues (brain and spinal cord), as previously described[17,18,66,67] with minor modifications. Briefly, single cells suspension was prepared from CNS tissues using mechanical digestion using 18G and 22G needles and enzymatic dissociation was done using Accumax (Innovative Cell Tech) and then, brain homogenates were passed through 100µM strainer to obtain single cell suspension. A 30% Percoll-density gradient was employed to remove myelin and mix-glial populations were collected from pellets. Cells were washed with PBS and used for further experimental analysis. To characterize phenotypic and functional states of immune cells flow cytometry assay was performed. The collected cells were re-suspended in 500 µL of FACS stain buffer. Cells were washed three times and re-suspended in 100 µl FACS stain buffer. To block non-specific binding, CD16/32 was added to samples and incubated on ice for 5 min in dark followed by addition of a number of surface antibodies as indicated for myeloid and lymphoid cells for 30 min at 4ºC in dark for flow cytometry. After incubations, cells were washed with FACS stain buffer, and fixed and permeabilized using Fixation/Permeabilization buffer set (Proteintech), as directed by the manufacturer instructions. After this, Intracellular staining of Antibodies (**Table 1**) directed against functional states of myeloid and lymphoid cells were done in permeabilization buffer for 1h at room temperature. After incubation, cells were washed 3 times with FACS buffer and run on ThermoFisher Attune cytometer and analyzed using FlowJo software. The flow cytometry gating strategy mentioned in supplementary (**Fig. S4**).

RNA isolation and quantitative PCR analysis

Trizol reagent was used to isolate RNA from spinal cord, spleen and bone-marrow-derived macrophage (BMDM) as per manufacturer's instructions. The RNA concentration and purity were determined using a Nanodrop spectrophotometer. RNA was reverse transcribed using the iScript cDNA Synthesis Kit (Biorad) according to the manufacturer's instructions. Using specific primers, mRNA expression of various genes associated with functional changes associated with immune cells, and primer directed against *Irg1* gene were quantified. The primer list is shown in the table (**Table 2**). The CFX Real-Time PCR Cycler (Biorad) was used to perform real-time qPCR. Using L-27 as an internal standard, relative mRNA expression was calculated using CFX maestro software (Biorad), and the relative amount of mRNA is presented in the form of fold change over control.

Immunoblotting analysis

The spinal cord, splenic cells, BMDM and different myeloid and lymphoid cells were lysed using protein lysis buffer containing protease inhibitor cocktail. Post 30 minutes of incubation, samples were centrifuged at 10,000 g for 20 min at 4°C. Protein estimation was done using Bradford assay. 30µg of protein was loaded on 4-20% gradient BioRad precast gel. Then, gel was transferred to the nitrocellulose membranes. After transferring, the membrane was blocked with 5% Skimmed Milk in TBST and incubated with indicated primary antibody for overnight at 4°C. Next day, the membranes were rinsed three times with TBST and incubated with the corresponding secondary antibody, at room temperature for 2 h. Post washing with TBST, the protein expression was visualized by adding ECL reagent (Thermo) and densiometric analysis was done by ImageJ software.

Adoptive transfer (Adt) and Recall experiments

The AdT experiment was performed as described before [66]. Briefly, Spleen and LNs were isolated and single cells were prepared followed by RBCs lysis. Further, single cell suspensions were restimulated with 20 µg/ml MOG_{35-55} peptide in the presence of anti-IFNγ (10ug/ml, BioXcell) and IL12p70 (20ng/ml) for 72hrs. After incubations, cells were harvested and washed, and 10 million cells were i.p. injected to B6 Wt mice. At day 0 and day 2, each mouse was administered with pertussis toxin. EAE scoring was done daily through traditional scoring method. For adoptive transfer experiment in Rag1 mice, CD4 T cells were isolated from both Wt and *Irg1* KO mice and restimulated as described above. Then, 10 million CD4 T cells were injected ip into Rag1 mice. For Recall response, spleen and LNs cells were isolated and were cultured with MOG_{35-55} peptide (20 ng/ml) and supernatant were collected at 48 hr, 72 hr and 96 hrs. The level of produced both

pro-inflammatory cytokines and anti-inflammatory cytokines were measured using elisa (Biolegend).

Analysis of immune response in *Irg1* KO mice

To analyze the inflammatory response, single cells were prepared from spleen/LNs and BILs were harvested from CNS tissues. Splenic/LNs cells and BILs were restimulated with MOG_{35-55} for 72 hrs and supernatant were collected for estimation cytokines production by Elisa. Cells were stimulated with PMA and Ionomycin for 4h. Then, cells were surface stained with FITC-CD4, and intracellular stained with anti-IL17a, anti-IFNγ, GM-CSF, T-bet, RORγt and IL4.

Generation of Bone Marrow Derived Macrophages (BMDMs)

Bone marrow derived macrophage were prepared as described before[66]. Bone marrow cells were flushed from femora and tibias of Wt and *Irg1* KO mice. After centrifugation, cells were cultured with complete RPMI-1640 containing 10% L-929 media for seven days with periodically fed with complete media. After seven days, cells were trypsinized and 1-2 million cells from each group seeded into new plate as indicated.

Chromatin immunoprecipitation (ChIP) assay: Chromatin immunoprecipitation (ChIP) assay was performed using Go-Chip-Grade Kit (Biolegend) as per manufacturer's instructions with slight modification. Briefly, 1% formaldehyde was directly added to cells to cross-link proteins with DNA, then, 10% glycine was added to neutralize the reaction. After this, cell pellets were collected using centrifuge at 2000rpm for 6min. Pellets were dissolved in sonication lysis buffer, and then pellets were broken into 200-bp pieces using Bioraptor plus (Diagenode). Collected fragments were incubated for an hour at 4°C in a shaker with Protein A/G magnetic beads (Selleckchem). Centrifuge was done, and pellets were incubated with either Anti-Mouse RORyt (Proteintech) or anti-mouse IgG (Proteintech) antibodies at 4°C overnight. After this, Protein A/G magnetic beads were added to Antibody-pellets complex for 1hr at 4°C with shaking. After incubation, the Antibody-Pellet complex was magnetically purified using magnetic separator. Then, 30 µL of eluent was added to antibody-DNA complexes for 30min. 20µl of 5M NaCl added to eluted samples and incubated at 65C for overnight to de-cross link the samples. The DNA was then purified using Biolegend kit. The DNA extracted from antibody-immunoprecipitated chromatin fragments was used in qPCR to amplify the fragment region of the binding sites on the IL17a promoter. The 5′-TAATTCCCCCACAAAGCAAC-3′ (forward) and 5′-TGAGGTCAGCACAGAACCAC-3′ (backward) primers were used to target the IL17a promoter sequences.

Statistical Analysis: GraphPad Version 10 for windows was used for statistical analysis. All data is expressed as mean standard deviation (SD), and one-way analysis of variance (ANOVA) and t- tests were used to determine statistical significance. Statistical significance was defined as a p-value of less than 0.05.

LEGENDS

Figure 1: *Irg1* expression is induced in the spinal cord of EAE mice.

A. Volcano plot showing RNA-seq results with significantly up (red dots) & downregulated genes (blue dots) with 8 hrs of LI treatment in comparison to untreated rat brain mixed glia, with the topmost 10 dysregulated genes labelled in black (Padj <0.0005 & logFC >1.5) (N=4). **B.** The *Irg1* expression was examined in rat brain mixed glia treated and untreated with LI at 4 hrs, 8 hrs and 16 hrs (N=3). (******* p $>10^{-6}$). **C.** qPCR and immunoblot data revealed the upregulation of *Irg1* (normalized with β-actin) in Spinal cord of EAE, Data are representative of three independent experiments. **D.** Representative images of spinal cord (CFA vs EAE) stained with *Irg1*, Bar graph representing the quantification of *Irg1* expression intensity as percentage of CFA from a total of three independent experiments. **E.** Quantitative analysis of *Irg1* expression in Monocytes, $CD4^+$cells, $CD11b^+$ macrophages as well as B-cells, presented as the relative protein expression normalized to housekeeping control β-actin, and expressed as fold change compared to CFA. **F.** qPCR analysis of *Irg1* expression in Monocytes, $CD4^+$cells, $CD11b^+$ macrophages as well as B-cells in CFA and EAE mice, normalized with the β-actin, and data represented from the three independent experiments. Data presents as bar graph are the mean ± SD. *p < 0.05, **p < 0.01, and ***p < 0.001 compared to LI or EAE group using student's t test, one-way ANOVA.

Figure 2: *Irg1* KO mice exhibited severe disease compared to Wild type (Wt) mice.

A. Wt and *Irg1* KO female mice were immunized with MOG_{35-55} (200 µg/mouse) on day 0 in CFA, and PT was given on days 0 and 2 of immunization. Clinical score was taken until 22 d (n = 22). **B.** Bar graph representing cumulative score of disease severity in Wt and *Irg1* KO mice (N=22). **C.** Recall response was done using ELISA assay of Spleen and LN isolated from Wt & *Irg1* KO mice (n=5) subjected to MOG (20 µg/ml) treatment, samples collected at 72 hrs and measured the level of IL17a, GM-CSF, IFNγ and IL4 cytokines with error bars representing the S.D (N=5). **D.** Representative images shows histopathological changes in the spinal cord tissues in EAE mice in Wt and *Irg1* KO groups at day 22 days post immunization. Sections were staind with hematoxilin and eosin (H&E) and Luxol fast blue to (LFB) to show cells infiltration and changes in myelin content. **E.** Flow cytometry analysis revealed the total count of CD45+ cells in the CNS of Wt and *Irg1* KO mice (N=5). **F.** Flow cytometry tSNE plot gated on $CD45^+$ cells in BILs from Wt and *Irg1* KO mice demonstrating myeloid cells populations; $CD11b^+$, $F4/80^+$, $Ly6C^+$, $CD11c^+$ populations. **G.** Flow cytometry analysis showing CD4+ populations in the CNS of Wt and *Irg1* KO mice (N=5). **H.** Representative flow cytometry tSNE plot of BILs gated on $CD4^+$ cells demonstrating IL17a, IFNγ, T-bet, RORγt and GM-CSF populations. **I.** Bar graph showing CD4+

cells expressing the total positive population of IL17a, IFNγ, GMCSF and as well as double positive (IL17-A+IFNγ) and triple positive (IL17-A+IFNγ+GMCSF) in Wt (n=5), and *Irg1* KO (n=5). **J.** Bar graph showing the total positive population of infiltrating macrophages, monocytes and dendritic cells. Data presents as bar graph are the mean ± SD. *p < 0.05, **p < 0.01, and ***p < 0.001 compared to *Irg1* KO group using student's t test, one-way ANOVA.

Figure 3: *Irg1* KO CD4 cells are highly pathogenic in nature.

A. (Left) Quantification of $CD4^+IL17a^+$ after $CD4^+$ cells from Wt and *Irg1* KO were adoptively transferred in B6 mice (N=5). **B.** Clinical score was taken until 17 d after B6 mice were immunized with MOG_{35-55} (200 µg/mouse) (N=10). **C.** Clinical score was taken in Rag1 mice after receiving adoptive transfer of $CD4^+$ cells from Wt and *Irg1* KO mice, following immunization with MOG_{35-55} (200 µg/mouse) and PT (n=10). Bar graph represents the positive populations of $CD4^+$ cells (**D**), $CD4^+IL17a^+$ cells (**E**), $CD4^+$ $IFNγ^+$ cells (**F**), $CD4^+$ $GMCSF^+$ cells (**G**), $CD4^+$ $IL4^+$ cells (**H**) and double positive ($IL17a^+IFNγ^+$) (**I**) cells in $CD4^+$ cells adoptively transferred cells from Wt and *Irg1* KO in Rag1 mice (N=4). **J**. Flow cytometry plot (left) gated on CD4+ cells showing double positive ($IL17a^+GMCSF^+$) populations in Rag1 mice which were presented as bar graph (right) (N=4). **K.** Flow cytometry plot (left) gated on CD4+ cells showing triple positive ($IL17a^+$ $IFNγ^+$ $GMCSF^+$) populations in Rag1 mice which were presented as bar graph (right) (N=4). NS not significant, *p < 0.05, **p < 0.01, and ***p < 0.001 compared to *Irg1* KO group using student's t test, one-way ANOVA.

Figure 4: Loss of *Irg1* pushes $CD4^+$ Cells towards more pathogenic Th17 subsets.

A. Representation of ELISA analysis of cytokine IL17a level in pathogenic and non-pathogenic Th17 cells isolated from Wt and *Irg1* KO mice (N=5). **B.** Representative flow cytometry plots (left) of $IL17a^+$ populations in npTh17 & pTh17 cells and data is presented as bar graph (right) showing $IL17a^+$ cells (MFI) in npTh17 and pTh17 cells (n=5). **C.** The heatmap showing mRNA expression of Th17 pathogenic and non-pathogenic signature genes in Wt and KO mice (N=3). **D.** An immunoblot data of RORγt (normalized with β-actin) in npTh17 and pTh17 cells of Wt and *Irg*1 KO. Data is representative of three independent experiments. **E.** Chip assay was performed to determine binding of RORγt on IL17a promoter. Data presented as a percentage fold of RORγt binding on IL17 promoter with respect to total input. Data is representative of three independent experiments. ***p < 0.001 compared to *Irg1* KO using student's t test, one-way ANOVA.

Figure 5: *Irg1* KO macrophages exhibit strong antigen presentation capability.

A. The levels of pro-inflammatory cytokines IL-6, TNFα, MCP-1 and IL1β in bone marrow derived macrophages (BMDM) of Wt and *Irg1* KO upon LPS stimulation for 6hrs (N=5). **B.** Bar graph represents mRNA expression of IL-6, TNFα and MCP-1 in BMDM of Wt and *Irg1* KO upon LPS stimulation for 6 hrs (N=5). **C.** Flow cytometry plots (left) of Class II$^+$ and CD86$^+$ populations in BMDM of Wt and KO upon IFNγ stimulation for 24hrs and quantifications of Class II$^+$ and CD86$^+$ cells with histogram overlay (right) of Class II$^+$ and CD86$^+$ cells between Wt and *Irg1* KO (n=5). **D.** Flow cytometry plot gated (left) on CD45^{hi+}CD11b$^+$F4/80$^+$ (infiltrated macrophages) showing Class II+ populations in Wt and *Irg1* KO and quantifications (right) of Class II$^+$ cells with histogram overlay of Class II$^+$ cells between Wt and *Irg1* KO (N=5). **E.** Representative flow cytometry tSNE plot (left) of BILs gated on CD45$^+$ cells demonstrating Class II$^+$ populations in Wt and *Irg1* KO mice and bar graph at right side showing populations of Class II expressing myeloid cells CD11b$^+$, F4/80$^+$, CD11c$^+$ and Ly6C$^+$ cells (N=5). **F.** Based on cell surface markers, bar graph represents populations of Class II expressing inflammatory DCs (CD45$^+$CD11c$^+$Class II$^+$), monocytic DCs (CD45$^+$CD11b$^+$CD11c$^+$Class II$^+$), infiltrated monocytes (CD45$^+$CD11b$^+$Ly6C$^+$Class II$^+$) and microglia cells (CD45^{low}CD11b$^+$Class II$^+$) (N=5). **$p < 0.01$, and ***$p < 0.001$ compared to *Irg1* KO group using student's t test, one-way ANOVA.

Figure 6: *Irg1* KO macrophages are more potent in pushing Wt CD4 T cells towards pTh17.

A. Schematic overview of co-culture study using Wt CD4 cells with Wt and *Irg1* KO macrophages. **B.** Bar graph represents data from ELISA assay demonstrating levels of pro-inflammatory cytokines released by Wt CD4 upon interactions with Wt and *Irg1* KO macrophages (N=5). **C.** Flow cytometry data (left) gated on CD4$^+$ cells demonstrating the populations of double positive (IL17a$^+$GM-CSF$^+$) upon coculture of Wt CD4 with Wt and *Irg1* KO macrophages and MFI values of positive populations of IL17a$^+$, GMCSF$^+$ and double positive (IL17a$^+$GM-CSF$^+$) are presented as a bar graph (right) (N=5). ***$p < 0.001$ compared to *Irg1* KO group using student's t test, one-way ANOVA.

Figure 7: IL1β plays role in antigen presentation of *Irg1* KO macrophages.

A. Representative flow cytometry tSNE plot gated on IL1β$^+$ cells demonstrating populations of IL1β producing various myeloid; CD11b$^+$, F4/80$^+$, CD11c$^+$, Ly6C$^+$ and Ly6G$^+$ cells. **B.** Bar graphs represent positive population of myeloid cells producing IL1β in Wt and *Irg1* KO mice. **C.** Heat map showing positive population of myeloid cells producing IL1β in Wt and *Irg1* KO mice (N=4). Bar graph represents total count of IL1β+ve expressing infiltrated macrophages

($CD45^{hi+}CD11b^{+}F4/80^{+}$) (**D**), microglial cells ($CD45^{low}CD11b^{+}$) (**E**), inflammatory DCs ($CD45^{+}CD11c^{+}ClassII^{+}$) (**F**), infiltrated DCs ($CD45^{+}CD11c^{+}$) (**G**), and monocytes ($CD45^{+}Ly6C^{+}Ly6G^{-}$) (**H**). Data presented here is mean + SD. **p < 0.01 and ***p < 0.001 compared to *Irg1* KO group using student's t test, one-way ANOVA.

Figure 8: Loss of *Irg1* KO exacerbated macrophage inflammation via NLRP3-IL1β mediated pathway.

A. Immunoblotting of Wt and *Irg1* KO macrophage stimulated with LPS for 4hr showing NLRP3, pro-IL1β, cleaved IL1β, ASC and GSDMD normalized with β-actin. **B.** Real-time quantitative PCR analysis of the fold change of NLRP3 and IL1β mRNA expression upon stimulation with LPS for 4hrs. **C.** Flow cytometry plot demonstrating populations of $IL17a^{+}$ and $IL17a^{+}GMCSF^{+}$ on $CD4^{+}$ cells upon co-culturing with Wt and *Irg1* KO macrophages in presence or absence of αIL1β (10 ng/ml). A population of $IL17a^{+}$ and double positive ($IL17a^{+}GMCSF^{+}$) CD4 cells presented as a bar graph after co-culturing of myelin-specific CD4 cells with Wt and *Irg1* KO macrophages in presence or absence of αIL1β (N=3). NS not significant, *p<0.05, **p<0.001, ***p<0.0001 compared to *Irg1* KO macrophages co-cultured with CD4 cells using student's t test, one-way ANOVA.

References:

1. Almolda, B., Gonzalez, B. & Castellano, B. Antigen presentation in EAE: role of microglia, macrophages and dendritic cells. *Front Biosci (Landmark Ed)* **16**, 1157-1171 (2011).
2. Chastain, E.M., Duncan, D.S., Rodgers, J.M. & Miller, S.D. The role of antigen presenting cells in multiple sclerosis. *Biochim Biophys Acta* **1812**, 265-274 (2011).
3. Loos, J.*, et al.* Functional characteristics of Th1, Th17, and ex-Th17 cells in EAE revealed by intravital two-photon microscopy. *J Neuroinflammation* **17**, 357 (2020).
4. Moser, T., Akgun, K., Proschmann, U., Sellner, J. & Ziemssen, T. The role of TH17 cells in multiple sclerosis: Therapeutic implications. *Autoimmun Rev* **19**, 102647 (2020).
5. Bomfim, C.C.B.*, et al.* Mycobacterium tuberculosis Induces Irg1 in Murine Macrophages by a Pathway Involving Both TLR-2 and STING/IFNAR Signaling and Requiring Bacterial Phagocytosis. *Front Cell Infect Microbiol* **12**, 862582 (2022).
6. Michelucci, A.*, et al.* Immune-responsive gene 1 protein links metabolism to immunity by catalyzing itaconic acid production. *Proc Natl Acad Sci U S A* **110**, 7820-7825 (2013).
7. Singh, S.*, et al.* Integrative metabolomics and transcriptomics identifies itaconate as an adjunct therapy to treat ocular bacterial infection. *Cell Rep Med* **2**, 100277 (2021).
8. Nair, S.*, et al.* Irg1 expression in myeloid cells prevents immunopathology during M. tuberculosis infection. *J Exp Med* **215**, 1035-1045 (2018).
9. Zhang, Z.*, et al.* Itaconate is a lysosomal inducer that promotes antibacterial innate immunity. *Mol Cell* **82**, 2844-2857 e2810 (2022).
10. Cordes, T.*, et al.* Immunoresponsive Gene 1 and Itaconate Inhibit Succinate Dehydrogenase to Modulate Intracellular Succinate Levels. *The Journal of biological chemistry* **291**, 14274-14284 (2016).
11. Lampropoulou, V.*, et al.* Itaconate Links Inhibition of Succinate Dehydrogenase with Macrophage Metabolic Remodeling and Regulation of Inflammation. *Cell Metab* **24**, 158-166 (2016).
12. Wu, R., Chen, F., Wang, N., Tang, D. & Kang, R. ACOD1 in immunometabolism and disease. *Cell Mol Immunol* **17**, 822-833 (2020).
13. Kuo, P.C.*, et al.* Dimethyl itaconate, an itaconate derivative, exhibits immunomodulatory effects on neuroinflammation in experimental autoimmune encephalomyelitis. *J Neuroinflammation* **17**, 138 (2020).
14. Aso, K.*, et al.* Itaconate ameliorates autoimmunity by modulating T cell imbalance via metabolic and epigenetic reprogramming. *Nat Commun* **14**, 984 (2023).

15. Fitzgerald, K.C.*, et al.* Multi-omic evaluation of metabolic alterations in multiple sclerosis identifies shifts in aromatic amino acid metabolism. *Cell Rep Med* **2**, 100424 (2021).
16. Mangalam, A.*, et al.* Profile of Circulatory Metabolites in a Relapsing-remitting Animal Model of Multiple Sclerosis using Global Metabolomics. *Journal of clinical & cellular immunology* **4**(2013).
17. Poisson, L.M.*, et al.* Untargeted Plasma Metabolomics Identifies Endogenous Metabolite with Drug-like Properties in Chronic Animal Model of Multiple Sclerosis. *The Journal of biological chemistry* **290**, 30697-30712 (2015).
18. Zahoor, I.*, et al.* Blood-based untargeted metabolomics in relapsing-remitting multiple sclerosis revealed the testable therapeutic target. *Proc Natl Acad Sci U S A* **119**, e2123265119 (2022).
19. Zahoor, I., Rui, B., Khan, J., Datta, I. & Giri, S. An emerging potential of metabolomics in multiple sclerosis: a comprehensive overview. *Cell Mol Life Sci* **78**, 3181-3203 (2021).
20. Chen, F.*, et al.* The STING1-MYD88 complex drives ACOD1/IRG1 expression and function in lethal innate immunity. *iScience* **25**, 104561 (2022).
21. Bartholomaus, I.*, et al.* Effector T cell interactions with meningeal vascular structures in nascent autoimmune CNS lesions. *Nature* **462**, 94-98 (2009).
22. Borges da Silva, H.*, et al.* Splenic Macrophage Subsets and Their Function during Blood-Borne Infections. *Front Immunol* **6**, 480 (2015).
23. Wagner, A.*, et al.* Metabolic modeling of single Th17 cells reveals regulators of autoimmunity. *Cell* **184**, 4168-4185 e4121 (2021).
24. El-Behi, M.*, et al.* The encephalitogenicity of T(H)17 cells is dependent on IL-1- and IL-23-induced production of the cytokine GM-CSF. *Nat Immunol* **12**, 568-575 (2011).
25. Komuczki, J.*, et al.* Fate-Mapping of GM-CSF Expression Identifies a Discrete Subset of Inflammation-Driving T Helper Cells Regulated by Cytokines IL-23 and IL-1beta. *Immunity* **50**, 1289-1304 e1286 (2019).
26. Codarri, L.*, et al.* RORgammat drives production of the cytokine GM-CSF in helper T cells, which is essential for the effector phase of autoimmune neuroinflammation. *Nat Immunol* **12**, 560-567 (2011).
27. Schnell, A., Littman, D.R. & Kuchroo, V.K. T(H)17 cell heterogeneity and its role in tissue inflammation. *Nat Immunol* **24**, 19-29 (2023).
28. Wu, B. & Wan, Y. Molecular control of pathogenic Th17 cells in autoimmune diseases. *Int Immunopharmacol* **80**, 106187 (2020).

29. Ivanov, II*, et al.* The orphan nuclear receptor RORgammat directs the differentiation program of proinflammatory IL-17+ T helper cells. *Cell* **126**, 1121-1133 (2006).
30. Yang, X.O.*, et al.* T helper 17 lineage differentiation is programmed by orphan nuclear receptors ROR alpha and ROR gamma. *Immunity* **28**, 29-39 (2008).
31. Bruck, W.*, et al.* Monocyte/macrophage differentiation in early multiple sclerosis lesions. *Ann Neurol* **38**, 788-796 (1995).
32. King, I.L., Dickendesher, T.L. & Segal, B.M. Circulating Ly-6C+ myeloid precursors migrate to the CNS and play a pathogenic role during autoimmune demyelinating disease. *Blood* **113**, 3190-3197 (2009).
33. Mildner, A.*, et al.* CCR2+Ly-6Chi monocytes are crucial for the effector phase of autoimmunity in the central nervous system. *Brain* **132**, 2487-2500 (2009).
34. Korn, T., Bettelli, E., Oukka, M. & Kuchroo, V.K. IL-17 and Th17 Cells. *Annu Rev Immunol* **27**, 485-517 (2009).
35. Chung, Y.*, et al.* Critical regulation of early Th17 cell differentiation by interleukin-1 signaling. *Immunity* **30**, 576-587 (2009).
36. Mufazalov, I.A.*, et al.* IL-1 signaling is critical for expansion but not generation of autoreactive GM-CSF+ Th17 cells. *EMBO J* **36**, 102-115 (2017).
37. Chu, F.*, et al.* The roles of macrophages and microglia in multiple sclerosis and experimental autoimmune encephalomyelitis. *J Neuroimmunol* **318**, 1-7 (2018).
38. Subhramanyam, C.S., Wang, C., Hu, Q. & Dheen, S.T. Microglia-mediated neuroinflammation in neurodegenerative diseases. *Semin Cell Dev Biol* **94**, 112-120 (2019).
39. Gris, D.*, et al.* NLRP3 plays a critical role in the development of experimental autoimmune encephalomyelitis by mediating Th1 and Th17 responses. *J Immunol* **185**, 974-981 (2010).
40. Inoue, M., Williams, K.L., Gunn, M.D. & Shinohara, M.L. NLRP3 inflammasome induces chemotactic immune cell migration to the CNS in experimental autoimmune encephalomyelitis. *Proc Natl Acad Sci U S A* **109**, 10480-10485 (2012).
41. Hooftman, A.*, et al.* The Immunomodulatory Metabolite Itaconate Modifies NLRP3 and Inhibits Inflammasome Activation. *Cell Metab* **32**, 468-478 e467 (2020).
42. Bambouskova, M.*, et al.* Itaconate confers tolerance to late NLRP3 inflammasome activation. *Cell Rep* **34**, 108756 (2021).
43. Rangachari, M. & Kuchroo, V.K. Using EAE to better understand principles of immune function and autoimmune pathology. *J Autoimmun* **45**, 31-39 (2013).

44. Jaiswal, A.K., *et al.* Irg1/itaconate metabolic pathway is a crucial determinant of dendritic cells immune-priming function and contributes to resolute allergen-induced airway inflammation. *Mucosal Immunol* **15**, 301-313 (2022).
45. Robinson, A.P., Harp, C.T., Noronha, A. & Miller, S.D. The experimental autoimmune encephalomyelitis (EAE) model of MS: utility for understanding disease pathophysiology and treatment. *Handb Clin Neurol* **122**, 173-189 (2014).
46. Chen, Y.J., *et al.* Targeting IRG1 reverses the immunosuppressive function of tumor-associated macrophages and enhances cancer immunotherapy. *Sci Adv* **9**, eadg0654 (2023).
47. Zhu, X., *et al.* Itaconic acid exerts anti-inflammatory and antibacterial effects via promoting pentose phosphate pathway to produce ROS. *Sci Rep* **11**, 18173 (2021).
48. Swain, A., *et al.* Comparative evaluation of itaconate and its derivatives reveals divergent inflammasome and type I interferon regulation in macrophages. *Nat Metab* **2**, 594-602 (2020).
49. Al-Mossawi, M.H., *et al.* Unique transcriptome signatures and GM-CSF expression in lymphocytes from patients with spondyloarthritis. *Nat Commun* **8**, 1510 (2017).
50. Choi, H.G., *et al.* Antigen-Specific IFN-gamma/IL-17-Co-Producing CD4(+) T-Cells Are the Determinants for Protective Efficacy of Tuberculosis Subunit Vaccine. *Vaccines (Basel)* **8**(2020).
51. Pishesha, N., Harmand, T.J. & Ploegh, H.L. A guide to antigen processing and presentation. *Nat Rev Immunol* **22**, 751-764 (2022).
52. Glatigny, S. & Bettelli, E. Experimental Autoimmune Encephalomyelitis (EAE) as Animal Models of Multiple Sclerosis (MS). *Cold Spring Harb Perspect Med* **8**(2018).
53. Zhao, Y., Liu, Z., Qin, L., Wang, T. & Bai, O. Insights into the mechanisms of Th17 differentiation and the Yin-Yang of Th17 cells in human diseases. *Mol Immunol* **134**, 109-117 (2021).
54. Mailer, R.K., *et al.* IL-1beta promotes Th17 differentiation by inducing alternative splicing of FOXP3. *Sci Rep* **5**, 14674 (2015).
55. Ronchi, F., *et al.* Experimental priming of encephalitogenic Th1/Th17 cells requires pertussis toxin-driven IL-1beta production by myeloid cells. *Nat Commun* **7**, 11541 (2016).
56. Hou, B., *et al.* Inhibition of the NLRP3-inflammasome prevents cognitive deficits in experimental autoimmune encephalomyelitis mice via the alteration of astrocyte phenotype. *Cell Death Dis* **11**, 377 (2020).

57. Mendiola, A.S. & Cardona, A.E. The IL-1beta phenomena in neuroinflammatory diseases. *J Neural Transm (Vienna)* **125**, 781-795 (2018).

58. Versele, R., Sevin, E., Gosselet, F., Fenart, L. & Candela, P. TNF-alpha and IL-1beta Modulate Blood-Brain Barrier Permeability and Decrease Amyloid-beta Peptide Efflux in a Human Blood-Brain Barrier Model. *Int J Mol Sci* **23**(2022).

59. Lopez-Castejon, G. & Brough, D. Understanding the mechanism of IL-1beta secretion. *Cytokine Growth Factor Rev* **22**, 189-195 (2011).

60. Mankan, A.K., Dau, T., Jenne, D. & Hornung, V. The NLRP3/ASC/Caspase-1 axis regulates IL-1beta processing in neutrophils. *Eur J Immunol* **42**, 710-715 (2012).

61. Xie, Q.M.*, et al.* Itaconate Suppresses the Activation of Mitochondrial NLRP3 Inflammasome and Oxidative Stress in Allergic Airway Inflammation. *Antioxidants (Basel)* **12**(2023).

62. Li, T.*, et al.* NLRP3 inflammasome-activating arginine-based liposomes promote antigen presentations in dendritic cells. *Int J Nanomedicine* **14**, 3503-3516 (2019).

63. Swanson, K.V., Deng, M. & Ting, J.P. The NLRP3 inflammasome: molecular activation and regulation to therapeutics. *Nat Rev Immunol* **19**, 477-489 (2019).

64. Yao, Y.*, et al.* Antigen-specific CD8(+) T cell feedback activates NLRP3 inflammasome in antigen-presenting cells through perforin. *Nat Commun* **8**, 15402 (2017).

65. Nicolas-Avila, J.A.*, et al.* A Network of Macrophages Supports Mitochondrial Homeostasis in the Heart. *Cell* **183**, 94-109 e123 (2020).

66. Mangalam, A.K.*, et al.* AMP-Activated Protein Kinase Suppresses Autoimmune Central Nervous System Disease by Regulating M1-Type Macrophage-Th17 Axis. *J Immunol* **197**, 747-760 (2016).

67. Suhail, H.*, et al.* An early glycolysis burst in microglia regulates mitochondrial dysfunction in oligodendrocytes under neuroinflammation. *iScience* **26**, 107921 (2023).

Figure 1

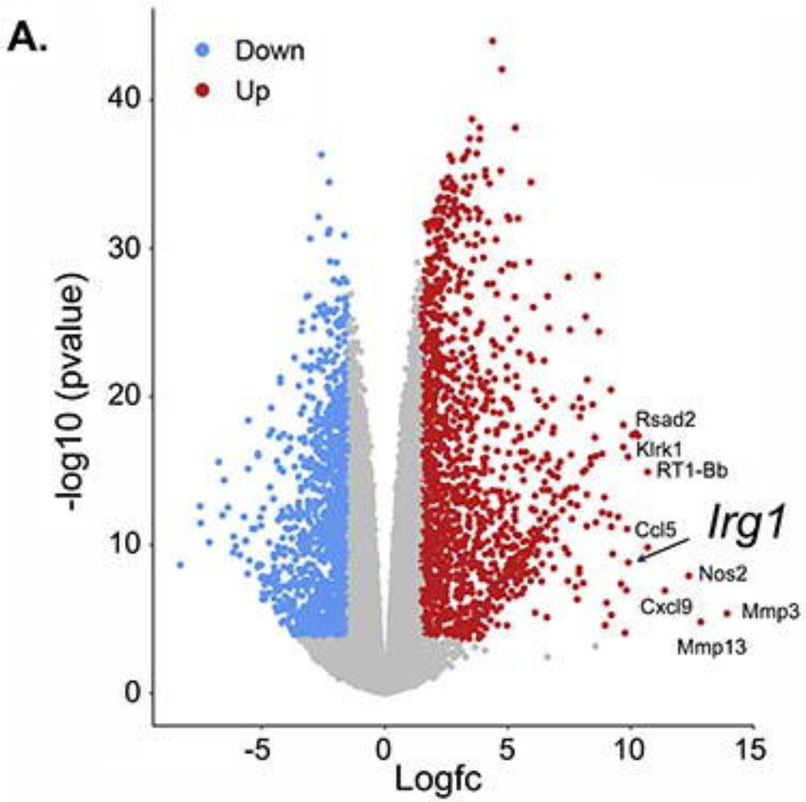
A.
Down
Up
-log10 (pvalue)
Logfc
Rsad2
Klrk1
RT1-Bb
Ccl5
Irg1
Nos2
Cxcl9
Mmp3
Mmp13

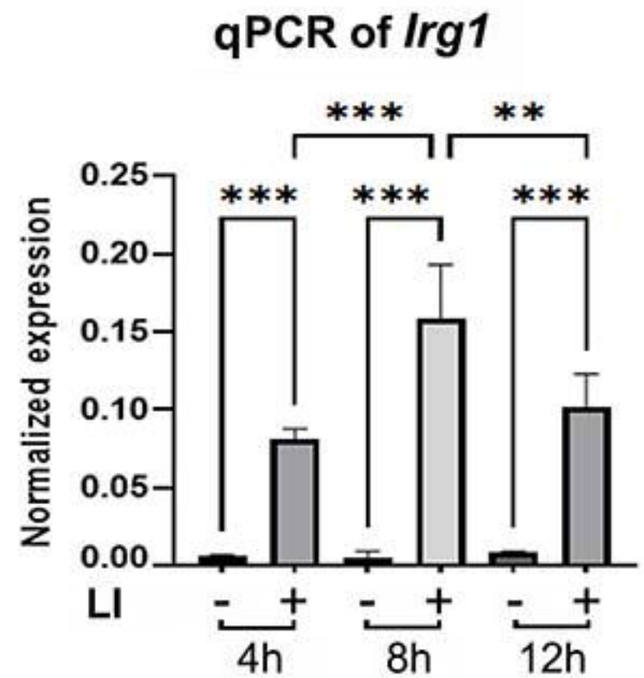
B.
qPCR of Irg1
Normalized expression
LI
4h
8h
12h

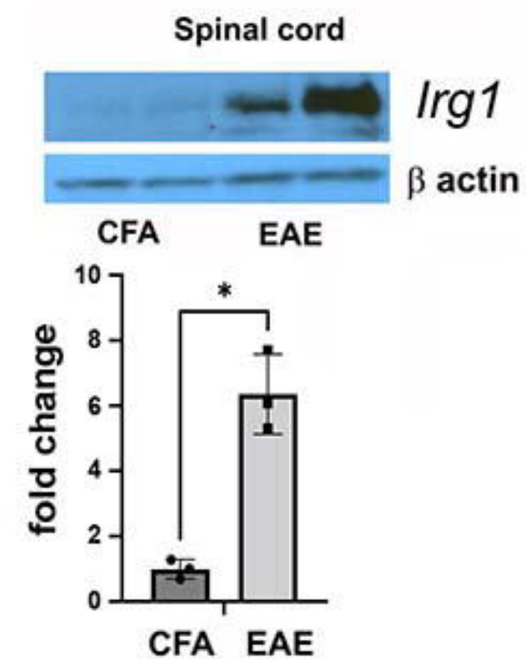
C.
Spinal cord
Irg1
β actin
CFA
EAE
fold change

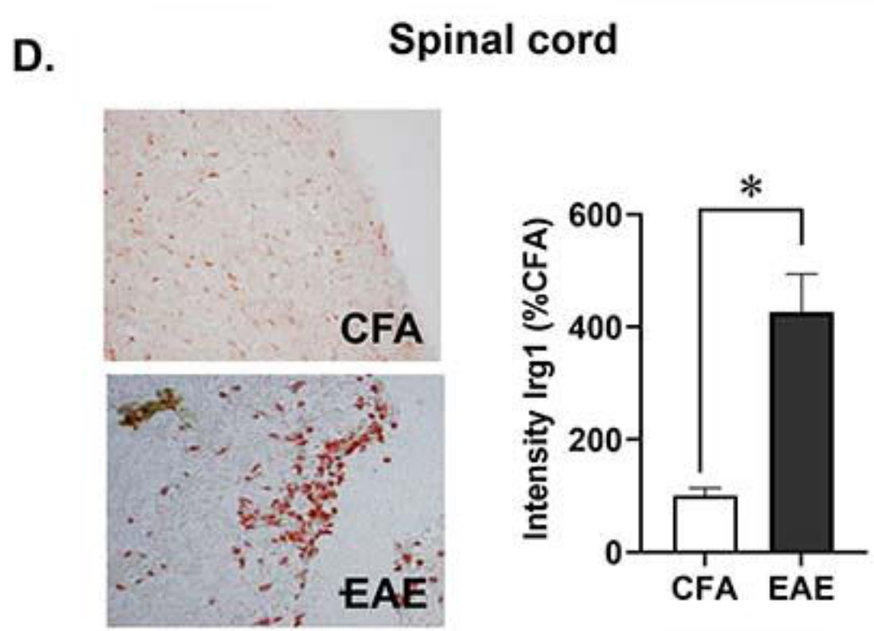
D.
Spinal cord
CFA
EAE
Intensity Irg1 (%CFA)

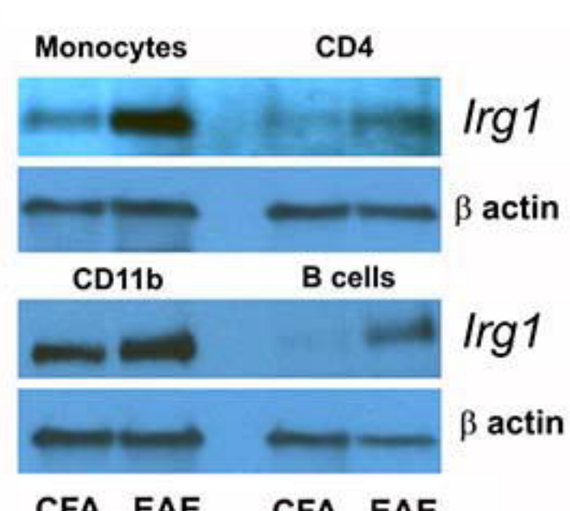
E.
Immunoblot analysis
Monocytes
CD4
Irg1
β actin
CD11b
B cells
CFA
EAE

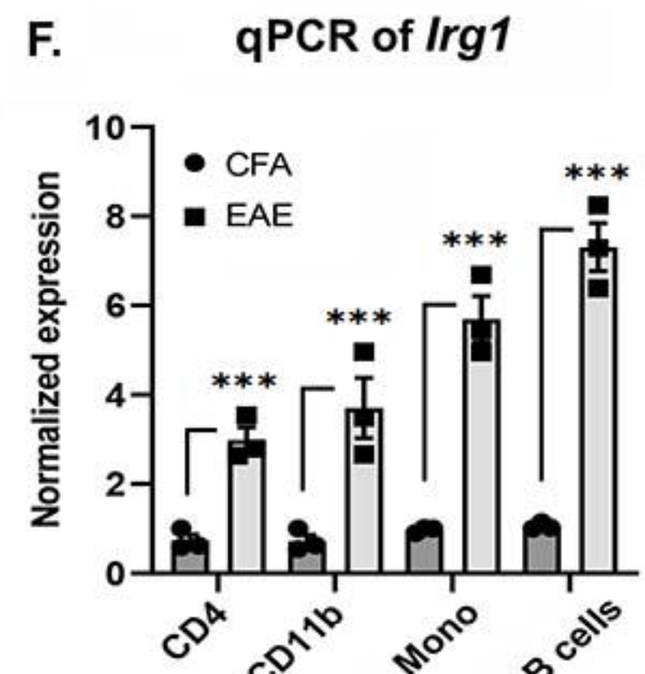
F.
qPCR of Irg1
CFA
EAE
Normalized expression
CD4
CD11b
Mono
B cells

Figure 2

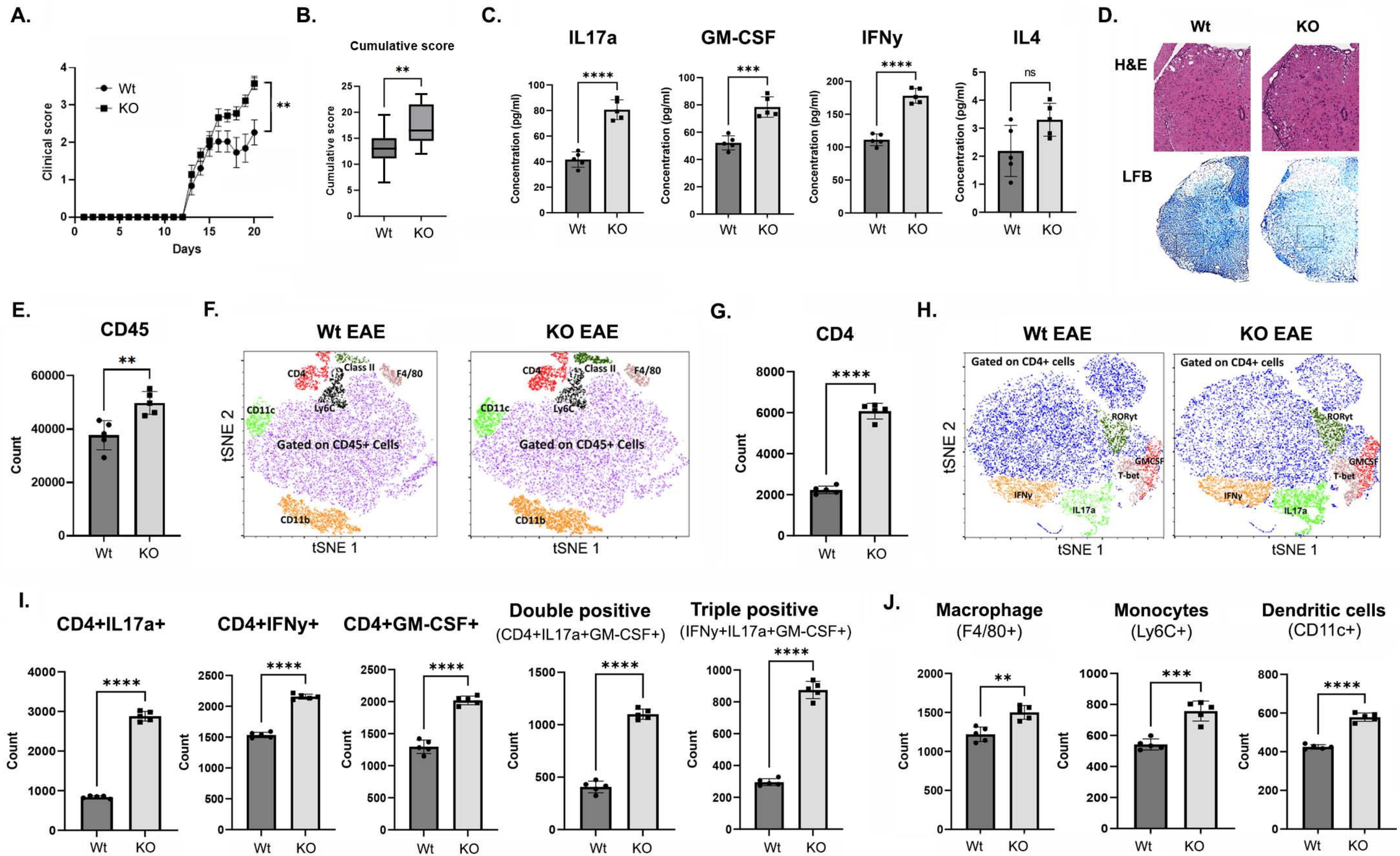
A.
Wt
KO
Clinical score
Days
**
B.
Cumulative score
Cumulative score
**
Wt
KO
C.
IL17a
GM-CSF
IFNy
IL4
Concentration (pg/ml)
****
***
****
ns
Wt
KO
D.
Wt
KO
H&E
LFB
E.
CD45
Count
**
Wt
KO
F.
Wt EAE
KO EAE
CD4
Class II
F4/80
CD11c
Ly6C
Gated on CD45+ Cells
CD11b
tSNE 1
tSNE 2
G.
CD4
Count
****
Wt
KO
H.
Wt EAE
KO EAE
Gated on CD4+ cells
RORγt
GMCSF
T-bet
IFNy
IL17a
tSNE 1
tSNE 2
I.
CD4+IL17a+
CD4+IFNy+
CD4+GM-CSF+
Double positive
(CD4+IL17a+GM-CSF+)
Triple positive
(IFNy+IL17a+GM-CSF+)
Count
****
Wt
KO
J.
Macrophage
(F4/80+)
Monocytes
(Ly6C+)
Dendritic cells
(CD11c+)
Count
**
***
****
Wt
KO

Figure 3

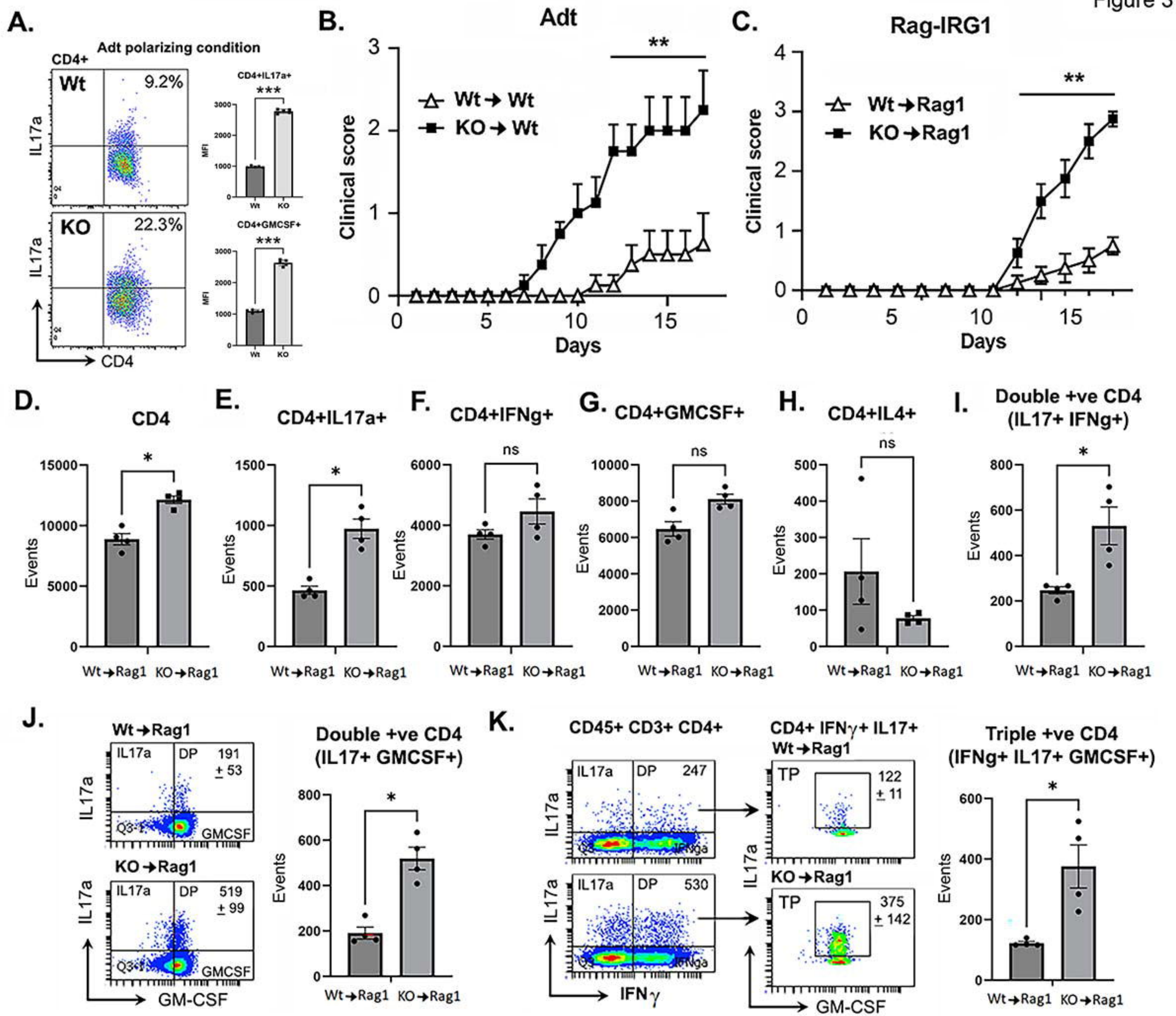
A.
Adt polarizing condition
CD4+
Wt
9.2%
KO
22.3%
IL17a
CD4
CD4+IL17a+
CD4+GMCSF+
***
MFI
Wt
KO
B.
Adt
Wt → Wt
KO → Wt
Clinical score
Days
**
C.
Rag-IRG1
Wt → Rag1
KO → Rag1
D.
CD4
E.
CD4+IL17a+
F.
CD4+IFNg+
G.
CD4+GMCSF+
H.
CD4+IL4+
I.
Double +ve CD4
(IL17+ IFNg+)
Events
ns
*
Wt → Rag1
KO → Rag1
J.
Wt → Rag1
IL17a
DP
191
± 53
GMCSF
KO → Rag1
519
± 99
GM-CSF
Double +ve CD4
(IL17+ GMCSF+)
K.
CD45+ CD3+ CD4+
247
530
IFNγ
CD4+ IFNγ+ IL17+
TP
122
± 11
375
± 142
Triple +ve CD4
(IFNg+ IL17+ GMCSF+)

Figure 4

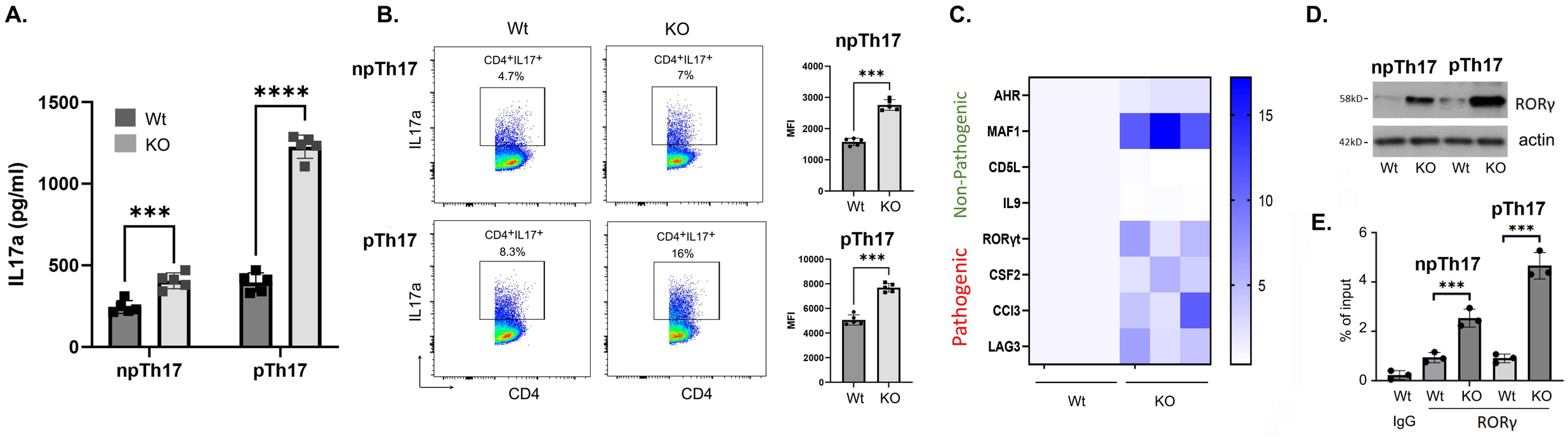
A.
IL17a (pg/ml)
1500
1000
500
0
Wt
KO
***
****
npTh17
pTh17
B.
Wt
KO
npTh17
pTh17
IL17a
CD4
CD4+IL17+
4.7%
7%
8.3%
16%
MFI
***
C.
Non-Pathogenic
Pathogenic
AHR
MAF1
CD5L
IL9
RORγt
CSF2
CCl3
LAG3
Wt
KO
15
10
5
D.
npTh17
pTh17
58kD
42kD
RORγ
actin
Wt
KO
E.
% of input
IgG
RORγ

Figure 5

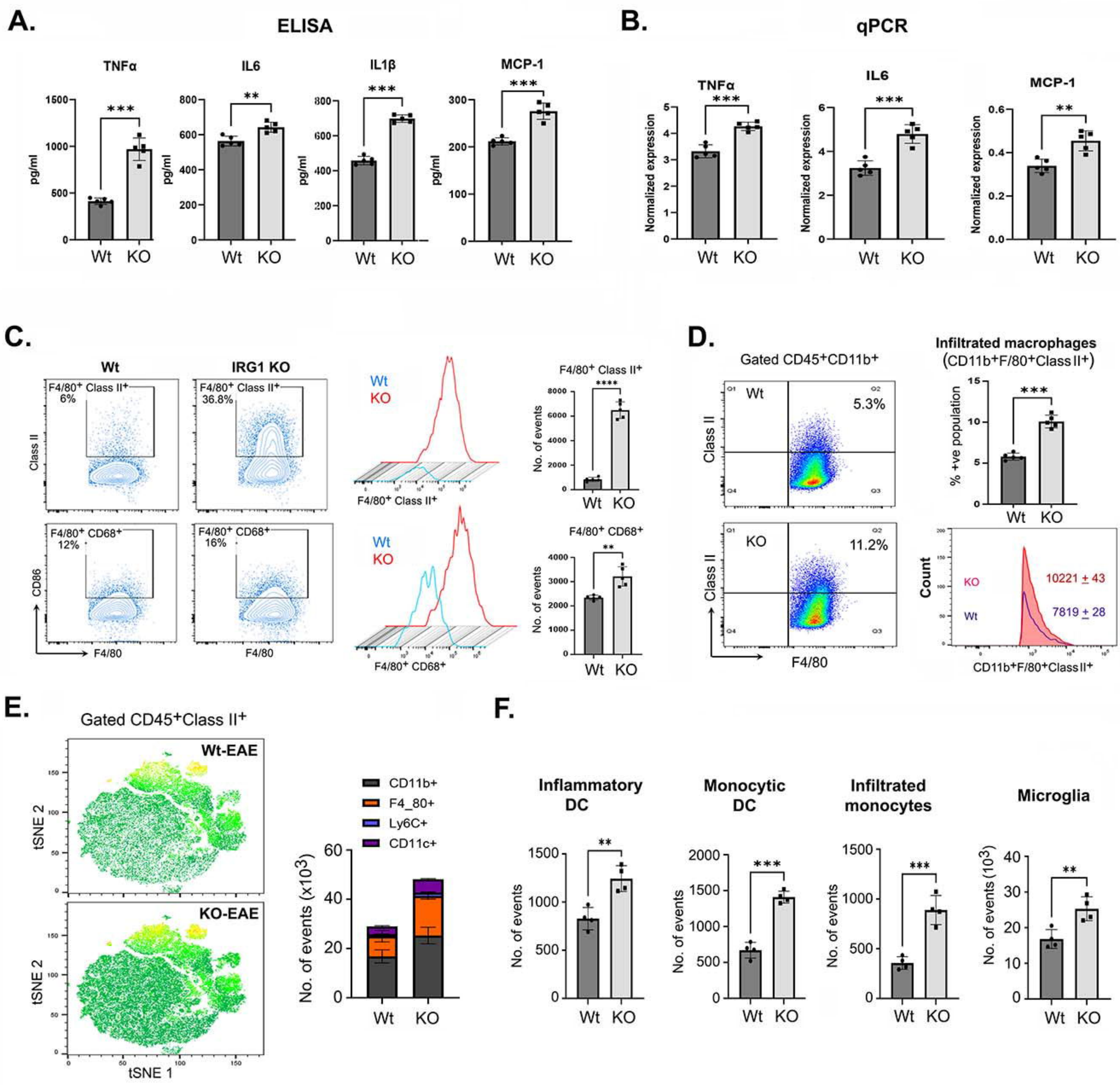
A.
ELISA
TNFα
IL6
IL1β
MCP-1
pg/ml
Wt
KO
B.
qPCR
Normalized expression
C.
Wt
IRG1 KO
F4/80+ Class II+
6%
36.8%
Class II
F4/80+ CD68+
12%
16%
CD86
F4/80
No. of events
D.
Gated CD45+CD11b+
Infiltrated macrophages
(CD11b+F/80+Class II+)
5.3%
11.2%
% +ve population
Count
10221 ± 43
7819 ± 28
CD11b+F/80+Class II+
E.
Gated CD45+Class II+
Wt-EAE
KO-EAE
tSNE 1
tSNE 2
CD11b+
F4_80+
Ly6C+
CD11c+
No. of events (x10^3)
F.
Inflammatory DC
Monocytic DC
Infiltrated monocytes
Microglia
No. of events (10^3)

Figure 6

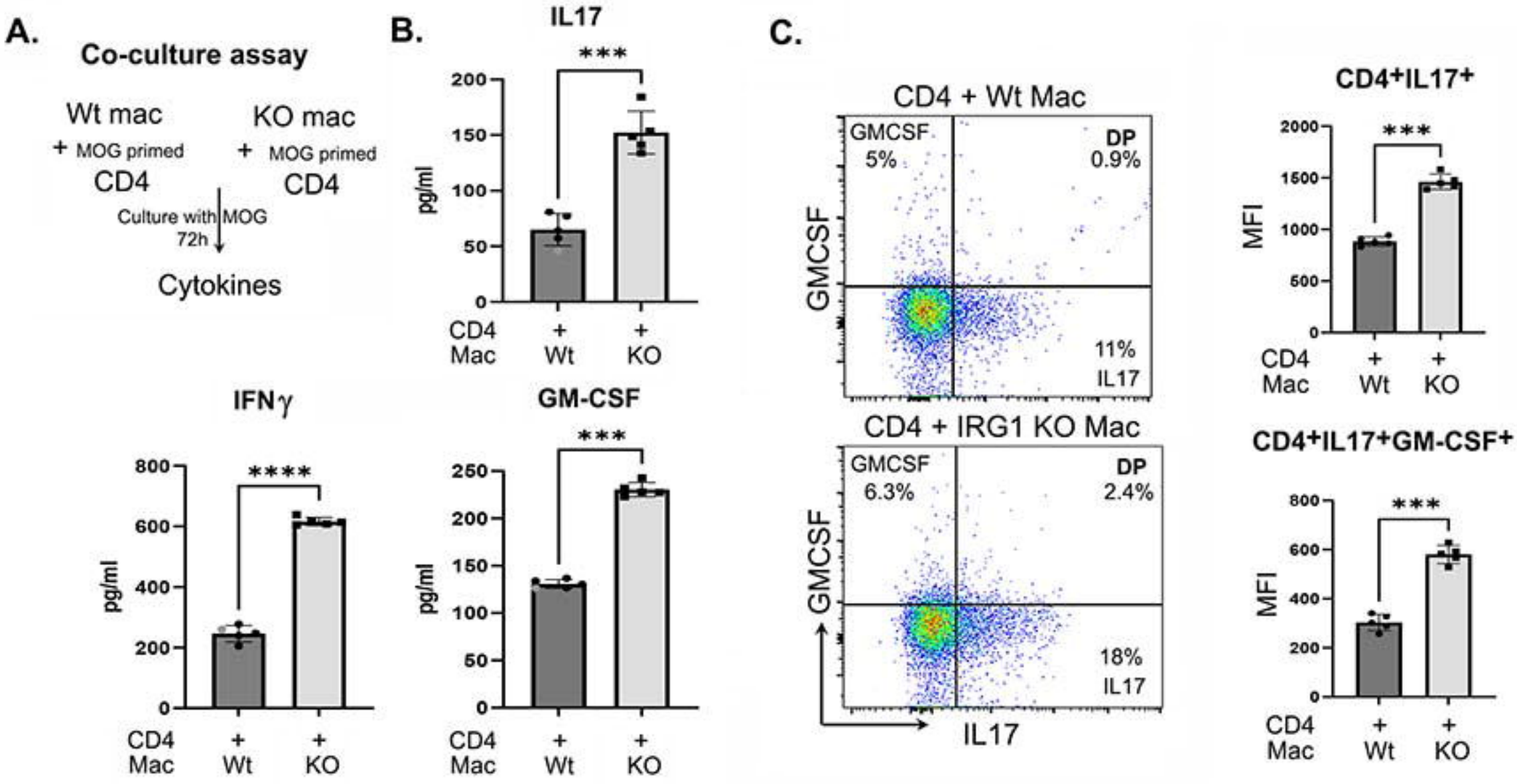
A.
Co-culture assay
Wt mac
+ MOG primed
CD4
KO mac
+ MOG primed
CD4
Culture with MOG
72h
Cytokines
B.
IL17
***
pg/ml
200
150
100
50
0
CD4
Mac
+
Wt
+
KO
IFNγ
****
800
600
400
200
0
GM-CSF
***
250
200
150
100
50
0
C.
CD4 + Wt Mac
GMCSF
5%
DP
0.9%
11%
IL17
CD4 + IRG1 KO Mac
GMCSF
6.3%
DP
2.4%
18%
IL17
GMCSF
IL17
CD4+IL17+
MFI
2000
1500
1000
500
0
CD4+IL17+GM-CSF+
800
600
400
200
0

Figure 7

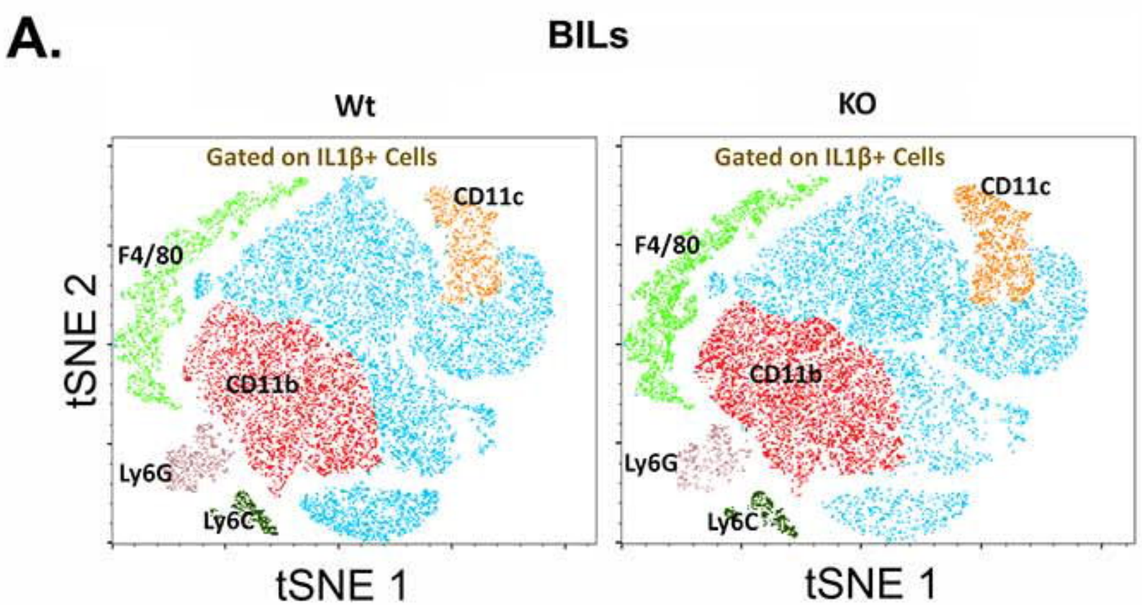
A.
BILs
Wt
KO
Gated on IL1β+ Cells
Gated on IL1β+ Cells
CD11c
F4/80
CD11b
Ly6G
Ly6C
tSNE 2
tSNE 1
tSNE 1

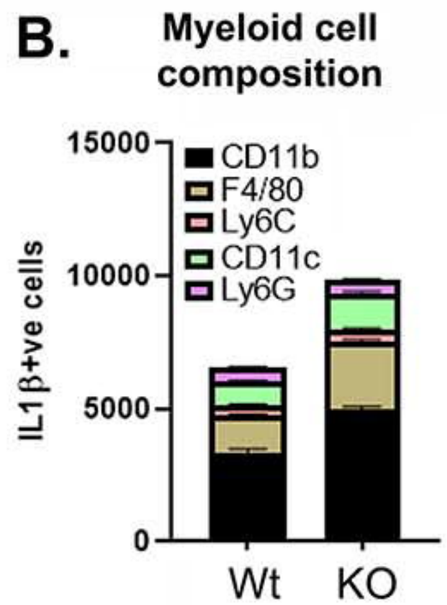
B.
Myeloid cell composition
CD11b
F4/80
Ly6C
CD11c
Ly6G
IL1β+ve cells
15000
10000
5000
0
Wt
KO

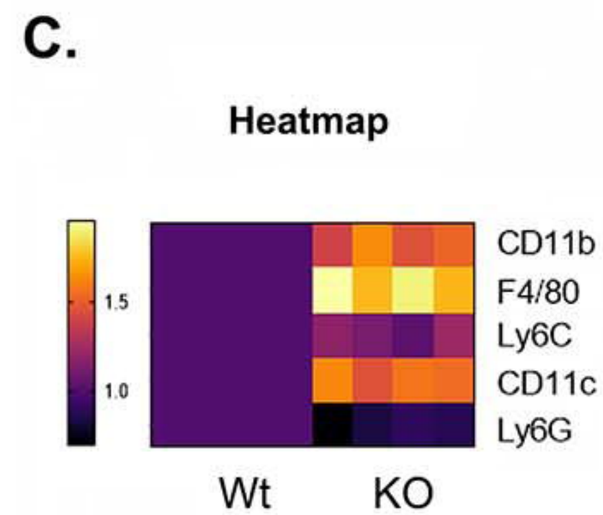
C.
Heatmap
1.5
1.0
CD11b
F4/80
Ly6C
CD11c
Ly6G
Wt
KO

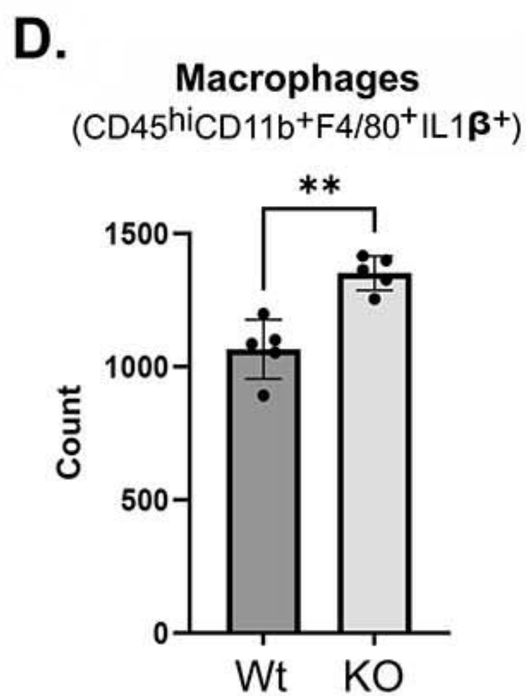
D.
Macrophages
(CD45hiCD11b+F4/80+IL1β+)
**
Count
1500
1000
500
0
Wt
KO

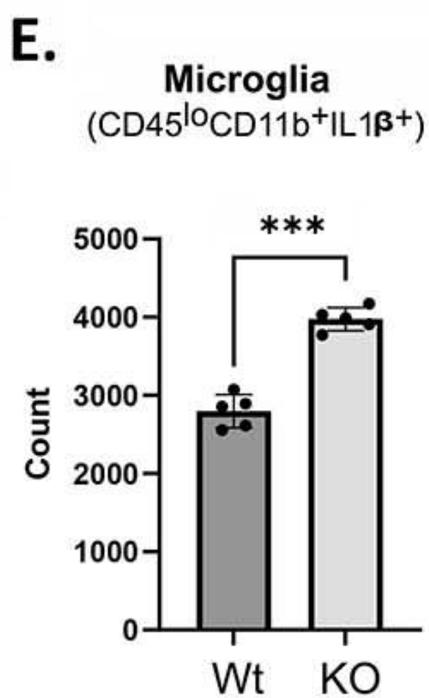
E.
Microglia
(CD45loCD11b+IL1β+)
***
Count
5000
4000
3000
2000
1000
0
Wt
KO

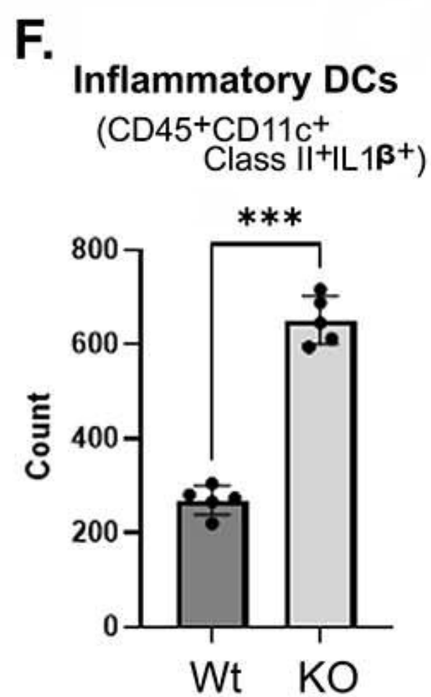
F.
Inflammatory DCs
(CD45+CD11c+
Class II+IL1β+)
***
Count
800
600
400
200
0
Wt
KO

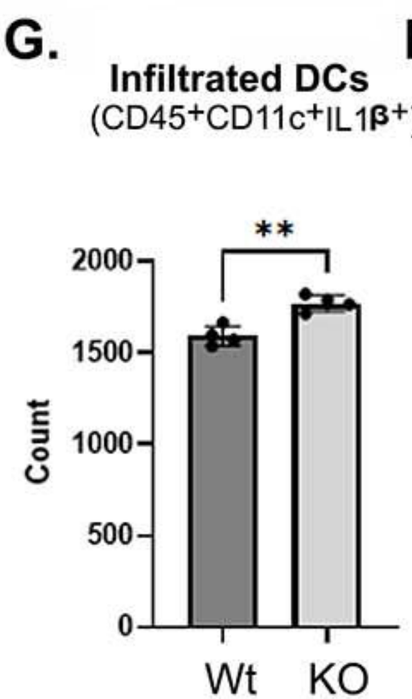
G.
Infiltrated DCs
(CD45+CD11c+IL1β+)
**
Count
2000
1500
1000
500
0
Wt
KO

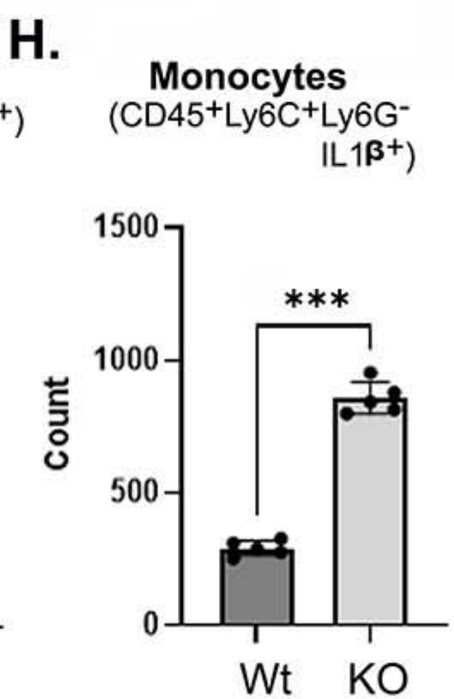
H.
Monocytes
(CD45+Ly6C+Ly6G-
IL1β+)
***
Count
1500
1000
500
0
Wt
KO

Figure 8

A.

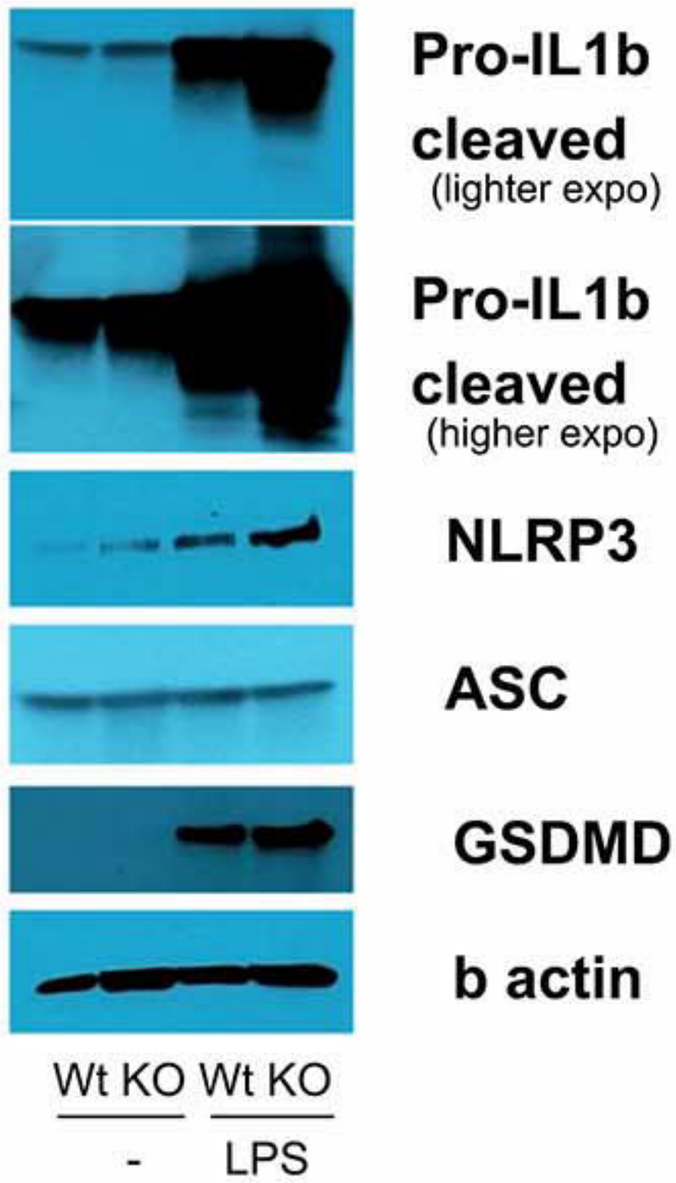
Pro-IL1b
cleaved
(lighter expo)
Pro-IL1b
cleaved
(higher expo)
NLRP3
ASC
GSDMD
b actin
Wt KO Wt KO
- LPS

B.

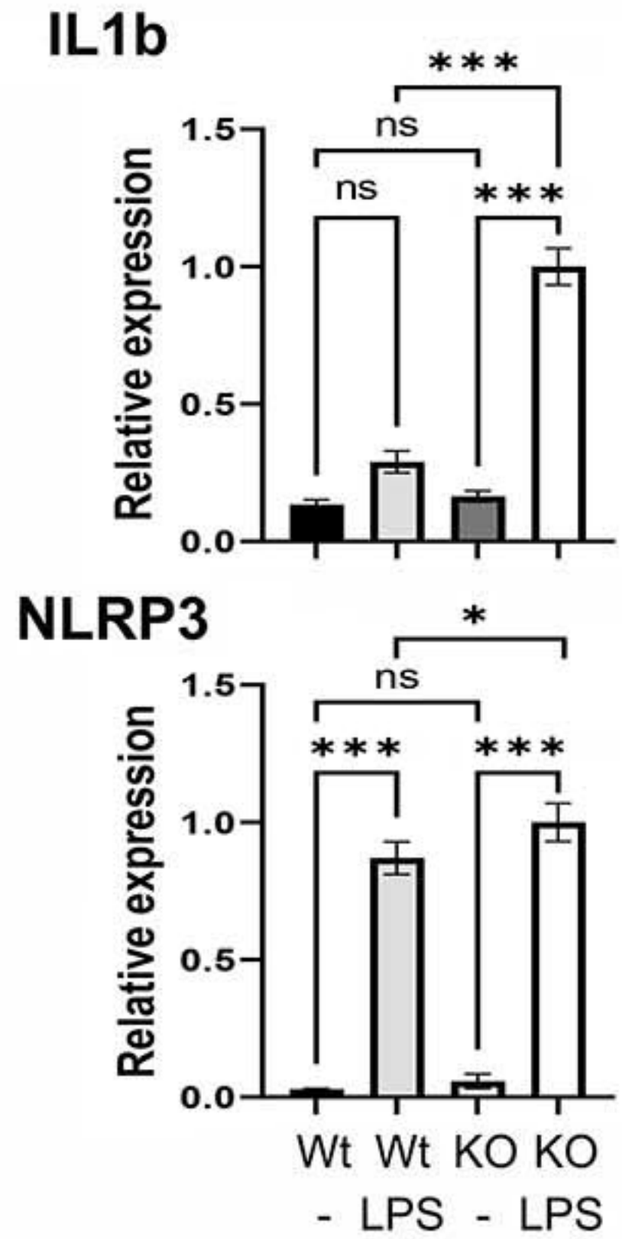
IL1b
Relative expression
1.5
1.0
0.5
0.0
ns
ns
***
***
NLRP3
Relative expression
1.5
1.0
0.5
0.0
*
ns
***
***
Wt Wt KO KO
- LPS - LPS

C.

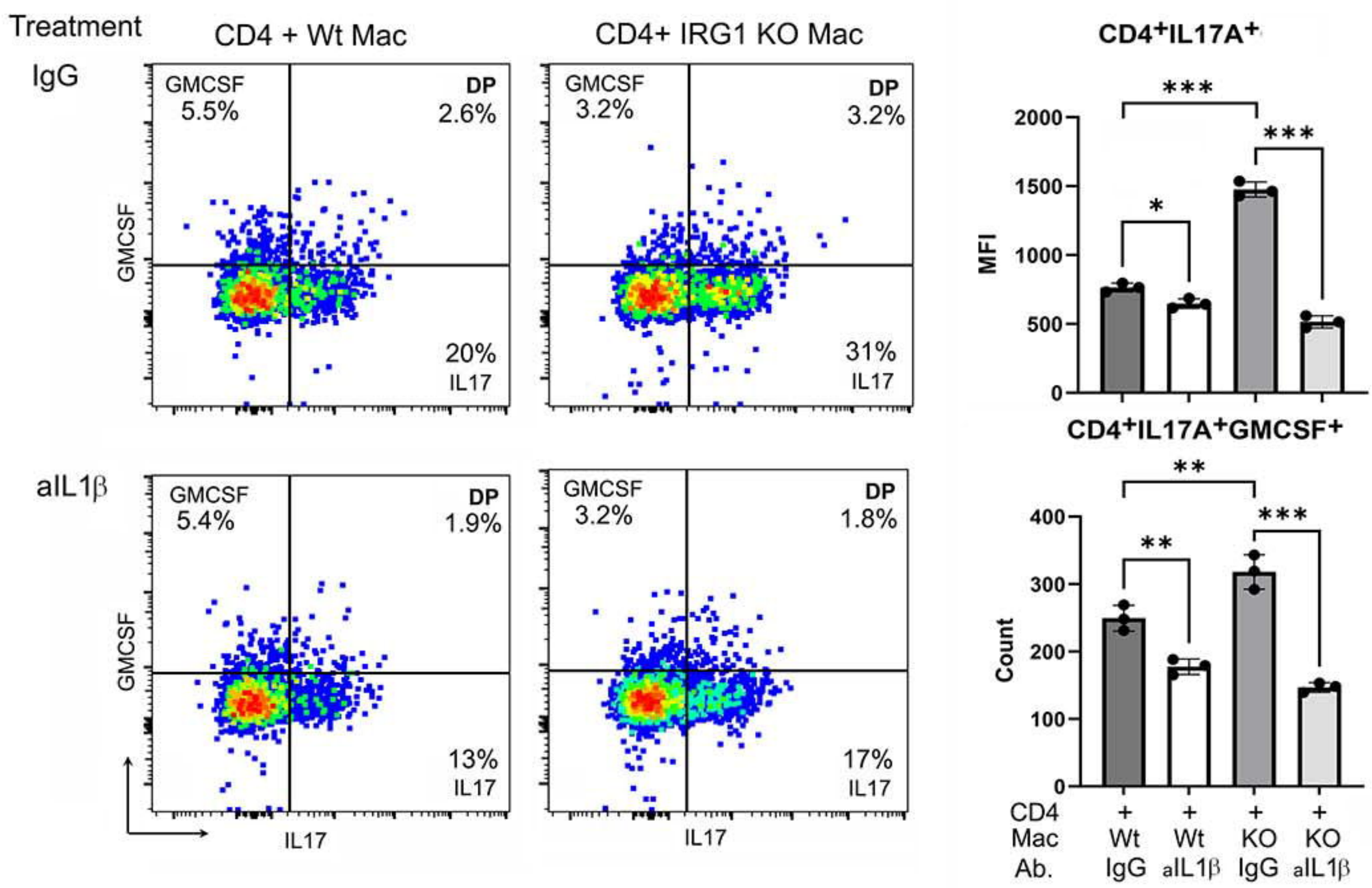
Treatment
CD4 + Wt Mac
CD4+ IRG1 KO Mac
IgG
GMCSF
5.5%
DP
2.6%
20%
IL17
GMCSF
3.2%
DP
3.2%
31%
IL17
aIL1β
GMCSF
5.4%
DP
1.9%
13%
IL17
GMCSF
3.2%
DP
1.8%
17%
IL17
GMCSF
IL17
CD4+IL17A+
MFI
2000
1500
1000
500
0
***
***
*
CD4+IL17A+GMCSF+
Count
400
300
200
100
0
**
**
***
CD4 + + + +
Mac Wt Wt KO KO
Ab. IgG aIL1β IgG aIL1β